Modelling and design of a subharmonically pumped K-band mixer

Piotr Przybyszewski
pip@pg.gda.pl
Supervisor: Dr Jerzy Chramiec
jec@pg.gda.pl
Supervisor at *ENSTB*: Jean Philippe Coupez
coupez@mot.enst-bretagne.fr

March, 1995

Contents

List of Tables

List of Figures

1 Preface

Design of a subharmonically pumped K band mixer with an anti-parallel pair of diodes is presented in this thesis. Modelling is split into nonlinear-linear and linear part. A nonlinear modelling tool – Kerr's reflection algorithm and a small signal analysis method are introduced. They are used in the nonlinear-linear analysis of the circuit. The results of nonlinear-linear analysis yield the conditions for the linear part of the project.

The filters are designed in uni-planar technology using distributed elements and modelled with ideal transmission lines, without considering influence of discontinuities and dispersion. The results of numerical optimization and measurements of the filter test circuits are presented. The results show very good agreement between simulation and measurements in the frequency band 0-40GHz.

Because of technical problems the diodes could not be mounted in the circuit. Therefore measured characteristics of the mixer are not presented in this thesis.

General concept and nonlinear-linear analysis of the mixer have been performed at the *Technical University of Gdańsk*. Modelling, realization and measurements of the passive elements of the mixer have been carried out at the *Ecole Nationale Supérieure des Télécommunications de Bretagne*, in Brest.

The *MDS-HP* software has been used in the modelling of the filters.

2 Introduction

2.1 Design specifications

A subharmonically pumped K band mixer intended to extend the bandwidth of *TEKTRONIX 2755* spectrum analyzer (see [1]).

Input bands:

- 20-30GHz
- 40-40GHz

Output band:

- 0-10GHz

LO **signal:**

- *Frequency:* approximately 15GHz
- *Available power:* $P_{LO} \leq 10\text{mW}$

Connectors:

- *Input port:* 50Ω *SSMA*. It enables direct coaxial line input for signals from 18–26.5GHz band, and waveguide input for signals from 26.5–40GHz using a rectangular waveguide – *SSMA* transition
- Output and *LO* ports: 50Ω *SMA* connectors

Nonlinear element:

- Anti-parallel pair of diodes

Conversion losses: Should be optimized. This parameter however, is not very important, since the mixer should work with relatively large input signals.

Uniplanar technology: Available substrates:

- *EPSILAM*, $\epsilon_r = 10.2$, $h = 635\mu m$, $t = 20\mu m$
- *Alumina*, $\epsilon_r = 9.9$, $h = 635\mu m$, $t = 10\mu m$
- *DUROID*, $\epsilon_r = 2.2$, $h = 256\mu m$, $t = 20\mu m$

3 Nonlinear-linear modelling

This section focuses on the nonlinear-linear part of the project. Large and small signal analysis of one diode circuits and circuits with an anti-parallel pair of diodes are presented in Sect. 3.1 and 3.2. The idea of a subharmonically pumped mixer is introduced in Sect. 3.3. Sect. 3.4 describes the diodes used in the project. Sect. 3.5 presents the numerical analysis of the nonlinear circuit.

In the nonlinear-linear analysis of the diode circuits we assume that the following conditions are satisfied:

- circuit has one harmonic source (and a polarisation source if necessary[1])
- circuit is in a steady state
- circuit is stable

3.1 Large signal analysis

3.1.1 Large signal analysis of one diode circuits

Fig. 1 shows the Thevenin's large signal model of a one diode circuit with one harmonic source $V_{LO}e^{j\omega_p t}$, V_{LO} being the source voltage magnitude, and ω_p denoting the source frequency.

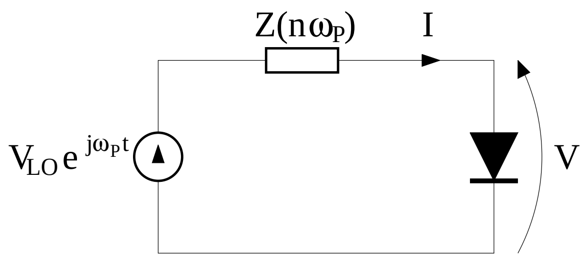

Figure 1: *Thevenin's large signal model of one diode circuits*

$I(t)$ and $V(t)$ on the diode may be represented in the form of the Fourier series:

$$I(t) = \sum_{n=-\infty}^{\infty} I_n e^{jn\omega_p t} \tag{1}$$

$$V(t) = \sum_{n=-\infty}^{\infty} V_n e^{jn\omega_p t} \tag{2}$$

From the Kirchoff's voltage law:

$$V_{LO}e^{j\omega_p t} = \sum_{n=-\infty}^{\infty} I_n Z(n\omega_p) e^{jn\omega_p t} + \sum_{n=-\infty}^{\infty} V_n e^{jn\omega_p t} \tag{3}$$

[1]It is not the case in this project, where an anti-parallel pair of diodes is used

Various methods may be used to calculate $I(t)$ and $V(t)$ waveforms, or I_n and V_n coefficients (see [2, pp. 91–101]). Kerr's reflection algorithm is used in this project. It is introduced in Sect. 3.5.1.

3.1.2 Large signal analysis of circuits with an anti-parallel pair of diodes

One diode model introduced in Sect. 3.1.1 may be used for analysis of many various configurations of diodes. Since we are going to work with an anti-parallel pair of diodes, the equivalent circuit will be shown for such a configuration.

Fig. 2 shows the Thevenin's large signal model of circuits with an anti-parallel pair of diodes.

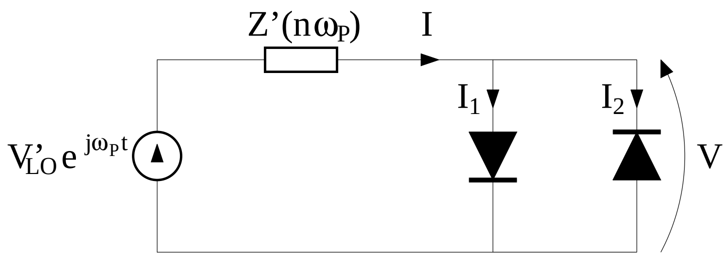

Figure 2: *Thevenin's large signal model of circuits with anti-parallel pair of diodes*

$V(t)$ and $I(t)$ are given by the Fourier series (2) and (1) respectively. The currents $I_1(t)$ and $I_2(t)$ are functions of $V(t)$. Since the diodes are connected in the anti-parallel configuration and it is assumed that they have the same characteristics, the following condition is satisfied:
If

$$I_1(t) = f_I(V(t)) \tag{4}$$

then

$$I_2(t) = -f_I(-V(t)) \tag{5}$$

Currents $I_1(t)$ and $I_2(t)$ may be expanded in the Fourier series:

$$I_1(t) = \sum_{n=-\infty}^{\infty} I_{1n} e^{jn\omega_p t} \tag{6}$$

$$\begin{aligned} I_2(t) &= \sum_{n=-\infty}^{\infty} I_{2n} e^{jn\omega_p t} = \\ &- \sum_{n=-\infty}^{\infty} I_{1n} e^{jn(\omega_p t - \pi)} \end{aligned} \tag{7}$$

From the Kirchoff's current law we get:

$$I(t) = I_1(t) + I_2(t) \tag{8}$$

or in the frequency domain:

$$I_n = I_{1n} + I_{2n} \tag{9}$$

From (6), (7) and (9) it follows that:

$$\begin{cases} \text{for odd } n: & I_{1n} = I_{2n} & \text{and} & I_n = 2I_{1n} \\ \text{for even } n: & I_{1n} = -I_{2n} & \text{and} & I_n = 0 \end{cases} \tag{10}$$

The circuit satisfies the Kirchoff's voltage law analogically to (3):

$$V'_{LO}e^{j\omega_p t} = \sum_{n=-\infty}^{\infty} I_n Z'(n\omega_p)e^{jn\omega_p t} + \sum_{n=-\infty}^{\infty} V_n e^{jn\omega_p t} \tag{11}$$

Using (10) the above relation becomes:

$$V'_{LO}e^{j\omega_p t} = \sum_{n'=-\infty}^{\infty} 2I_{2n'+1}Z'((2n'+1)\omega_p)e^{j(2n'+1)\omega_p t} + \sum_{n=-\infty}^{\infty} V_n e^{jn\omega_p t} \tag{12}$$

Comparing (12) and (3) we may construct an equivalent one diode model with the parameters:

$$Z(n\omega_p) = \begin{cases} 2Z'(n\omega_p) & \text{for odd } n \\ 0 & \text{for even } n \end{cases} \tag{13}$$

and

$$V_{LO} = V'_{LO} \tag{14}$$

(see Fig. 3).

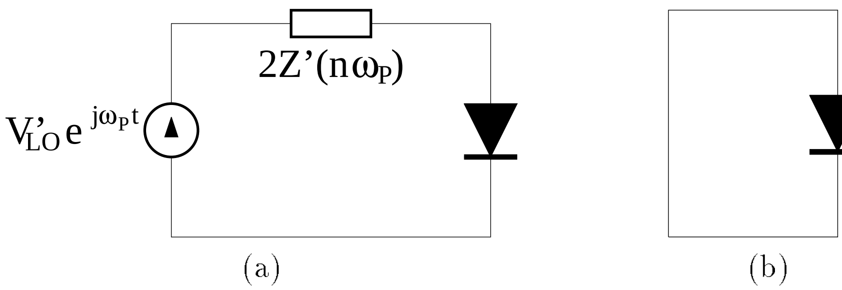

Figure 3: *Equivalent large signal one diode model for the circuit with an anti-parallel pair of diodes. Odd (a) and even harmonics (b).*

The available local oscillator power of the equivalent circuit is:

$$P_{LO} = \frac{V_{LO}}{8\Re[Z(\omega_p)]} = \frac{V'_{LO}}{8\Re[2Z'(\omega_p)]} = \frac{P'_{LO}}{2} \tag{15}$$

3.2 Small signal analysis

3.2.1 Small signal analysis of one diode circuits

In the large signal analysis of the diode circuits (Sect. 3.1) we have assumed that there was only one input signal. Here we will see what happens in the circuit, when additional small input signal is applied.

Variations of the diode current, caused by the additional voltage signal may be expressed by the Taylor series:

$$\begin{aligned} I(V+v) &= f_I(V+v) = \\ & f_I(V) + \left.\frac{\partial f_I}{\partial v'}\right|_{v'=V} v + \frac{1}{2!}\left.\frac{\partial^2 f_I}{\partial v'^2}\right|_{v'=V} v^2 + ... \end{aligned} \tag{16}$$

where $V = V(t)$ is a large input signal, and $v = v(t)$ is an additional small signal. With the assumption $V \gg v$:

$$I(V+v) - I(V) \simeq \left.\frac{\partial f_I}{\partial v'}\right|_{v'=V} v = g(t) \cdot v \tag{17}$$

where g(t) is the small signal parametric conductance:

$$g(t) = \left.\frac{\partial I}{\partial v'}\right|_{v'=V(t)} \tag{18}$$

If the diode is pumped with one harmonic source, then V(t) is given by (2) and $g(t)$ may be expressed as a Fourier series:

$$g(t) = \sum_{n=-\infty}^{\infty} G_n e^{jn\omega_p t} \tag{19}$$

where ω_p is the source frequency.

Analogical approach may be used for small signal parametric capacitance giving its time representation:

$$c(t) = \left.\frac{\partial Q}{\partial v'}\right|_{v'=V(t)} \tag{20}$$

with Q denoting large signal charge. The Fourier series representation of $c(t)$ is:

$$c(t) = \sum_{n=-\infty}^{\infty} C_n e^{jn\omega_p t} \tag{21}$$

Fig. 4 shows the Thevenin's small signal model of a one diode circuit. Fig. 5 shows an equivalent Norton's model.

Thevenin's and Norton's circuits are related by equations:

$$I_S = V_S \cdot Z(\omega_s + K\omega_p) \tag{22}$$

$$Y(\omega_s + m\omega_p) = [Z(\omega_s + m\omega_p)]^{-1} \tag{23}$$

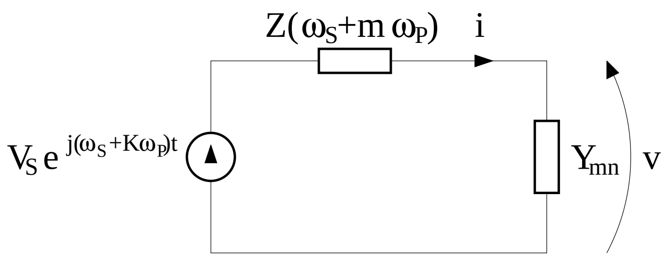

Figure 4: *Thevenin's small signal model of one diode circuit*

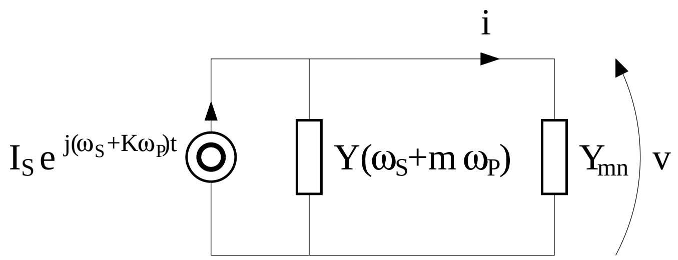

Figure 5: *Norton's small signal model of one diode circuit*

The diode is represented by parametric admittance Y_{mn}. We will represent Y_{mn} with coefficients G_n and C_n .

For the small-signal analysis the diode is no longer treated as a nonlinear element, but as a linear time-variable conductance ($g(t)$) and capacitance ($c(t)$). Then:

$$\begin{aligned} i(t) &= g(t)v(t) + \frac{d(c(t)v(t))}{dt} = \\ & g(t)v(t) + \frac{dc(t)}{dt}v(t) + c(t)\frac{v(t)}{dt} \end{aligned} \tag{24}$$

The small voltage $v(t)$ and current $i(t)$ signals may be expressed in the series form:

$$v(t) = \sum_{n=-\infty}^{\infty} V_{Sn} e^{j(\omega_s + n\omega_p)t} \tag{25}$$

$$i(t) = \sum_{n=-\infty}^{\infty} I_{Sn} e^{j(\omega_s + n\omega_p)t} \tag{26}$$

Equation (24) may be then expressed as a series:

$$\begin{aligned} & \sum_{k=-\infty}^{\infty} I_{Sk} e^{j(\omega_s + k\omega_p)t} = \sum_{m=-\infty}^{\infty} \sum_{n=-\infty}^{\infty} G_m V_{Sn} e^{j[\omega_s + (m+n)\omega_p]t} + \\ & \sum_{m=-\infty}^{\infty} \sum_{n=-\infty}^{\infty} j[\omega_s + (m+n)\omega_p] C_m V_{Sn} e^{j[\omega_s + (m+n)\omega_p]t} = \\ & \sum_{m=-\infty}^{\infty} \sum_{n=-\infty}^{\infty} Y_{mn} V_{Sn} e^{j[\omega_s + (m+n)\omega_p]t} \end{aligned} \tag{27}$$

where:

$$Y_{mn} = G_m + j[\omega_s + (m+n)\omega_p]C_m \tag{28}$$

From the Kirchoff's current law applied to the Norton's model we get:

$$\begin{aligned} I_S e^{j(\omega_s + K\omega_p)t} &= \sum_{m=-\infty}^{\infty} Y(\omega_s + m\omega_p) V_{Sm} e^{jk(\omega_s + m\omega_p)t} + \\ &\sum_{m=-\infty}^{\infty} \sum_{n=-\infty}^{\infty} Y_{mn} V_{Sn} e^{jk[\omega_s + (m+n)\omega_p]t} \end{aligned} \tag{29}$$

Comparing the coefficients at the same $e^{jk\omega_p t}$ terms in (29) we have:

$$Y(\omega_s + k\omega_p)V_{Sk} + \sum_{m=-\infty}^{\infty} Y_{m(k-m)} V_{S(k-m)} = \begin{cases} I_S & \text{for} \quad k = K \\ 0 & \text{for} \quad k \neq K \end{cases} \tag{30}$$

where the unknowns are complex voltage magnitudes V_{Sn} at frequencies $\omega_n = \omega_s + n\omega_p$. Equation (30) describes mixer in a steady state.

3.2.2 Small signal analysis of circuits with anti-parallel pair of diodes

Fig. 6 shows the Thevenin's small signal model of circuits with an anti-parallel pair of diodes . Fig. 7 shows an equivalent Norton's model.

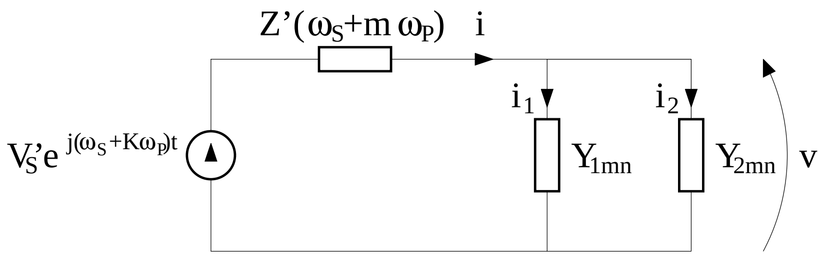

Figure 6: *Thevenin's small signal model of circuits with anti-parallel pair of diodes*

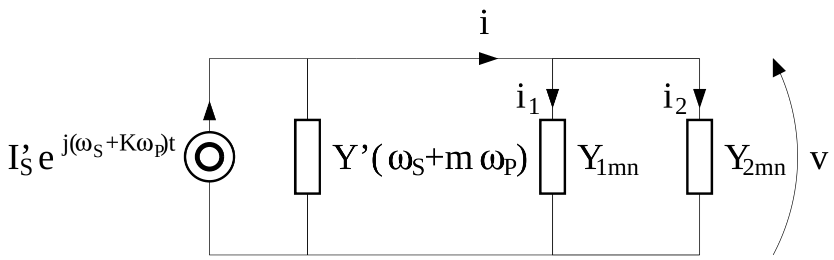

Figure 7: *Norton's small signal model of circuits with anti-parallel pair of diodes*

Both circuits are related by equations analogical to (22) and (23). Two diodes are represented by parametric admittances Y_{1mn} and Y_{2mn}. We will show that the small signal model of the circuit with an anti-parallel pair of diodes may be replaced by an equivalent one diode model.

Dynamic conductances g_1 and g_2 are functions of large voltage signal $V(t)$, and since the diodes have the same characteristics, the following condition is satisfied:
If

$$g_1(t) = f_g(V(t)) \tag{31}$$

then

$$g_2(t) = f_g(-V(t)) \tag{32}$$

Conductances $g_1(t)$ and $g_2(t)$ may be expanded in a Fourier series:

$$g_1(t) = \sum_{n=-\infty}^{\infty} G_{1n} e^{jn\omega_p t} \tag{33}$$

$$\begin{aligned} g_2(t) &= \sum_{n=-\infty}^{\infty} G_{2n} e^{jn\omega_p t} = \\ & \sum_{n=-\infty}^{\infty} G_{1n} e^{jn(\omega_p t - \pi)} \end{aligned} \tag{34}$$

The analogical analysis may be performed for dynamic capacitances $c_1(t)$ and $c_2(t)$ with coefficients C_{1n} and C_{2n} in the Fourier series respectively. Hence, $c_2(t)$ may be expressed, like $g_2(t)$, but with coefficients C_{1n}:

$$\begin{aligned} c_2(t) &= \sum_{n=-\infty}^{\infty} C_{2n} e^{jn\omega_p t)} = \\ & \sum_{n=-\infty}^{\infty} C_{1n} e^{jn(\omega_p t - \pi)} \end{aligned} \tag{35}$$

Like in (28) complex parametric admittances of each diode in a circuit may be expressed with $G_{1,2mn}$ and $C_{1,2mn}$ coefficients:

$$Y_{1,2mn} = G_{1,2m} + j[\omega_s + (m+n)\omega_p] C_{1,2m} \tag{36}$$

The small signal admittance of an anti-parallel pair of diodes is:

$$Y_{mn} = Y_{1mn} + Y_{2mn} \tag{37}$$

From (34), (35), (36) and (37):

$$\left\{ \begin{array}{lll} \text{for odd } m\text{:} & Y_{1mn} = -Y_{2mn} & \text{and} \quad Y_{mn} = 0 \\ \text{for even } m\text{:} & Y_{1mn} = Y_{2mn} & \text{and} \quad Y_{mn} = 2Y_{1mn} \end{array} \right. \tag{38}$$

Analogically to (30), we have:

$$Y'(\omega_s + k\omega_p) V_{sk} + \sum_{m=-\infty}^{\infty} Y_{m(k-m)} V_{S(k-m)} = \left\{ \begin{array}{lll} I'_S & \text{for} & k = K \\ 0 & \text{for} & k \neq K \end{array} \right. \tag{39}$$

where K denotes the input signal index ($I'_S e^{\omega_s + K\omega_p}$).

Putting (38) into (39) and dividing both sides of the equation by 2 we have:

$$\frac{Y'(\omega_s + k\omega_p)}{2} \cdot V_{Sk} + \sum_{m'=-\infty}^{\infty} Y_{2m'(k-m')} V_{S(k-2m')} = \begin{cases} \frac{I'_S}{2} & \text{for} \quad k = K \\ 0 & \text{for} \quad k \neq K \end{cases} \tag{40}$$

Comparing (40) with (30) we may construct an equivalent one diode small signal model with the following impedances:

$$Z(\omega_s + m\omega_p) = \begin{cases} 0 & \text{for even } m \\ 2Z'(\omega_s + m\omega_p) & \text{for odd } m \end{cases} \tag{41}$$

(see Fig. 8).

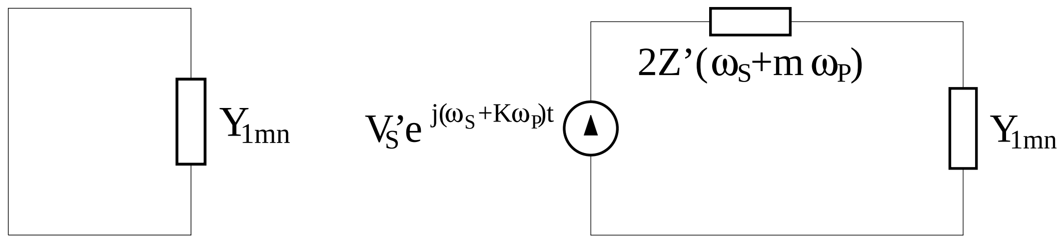

Figure 8: *Equivalent small signal one diode model of circuit with anti-parallel pair of diodes. Odd (a) and even m (b).*

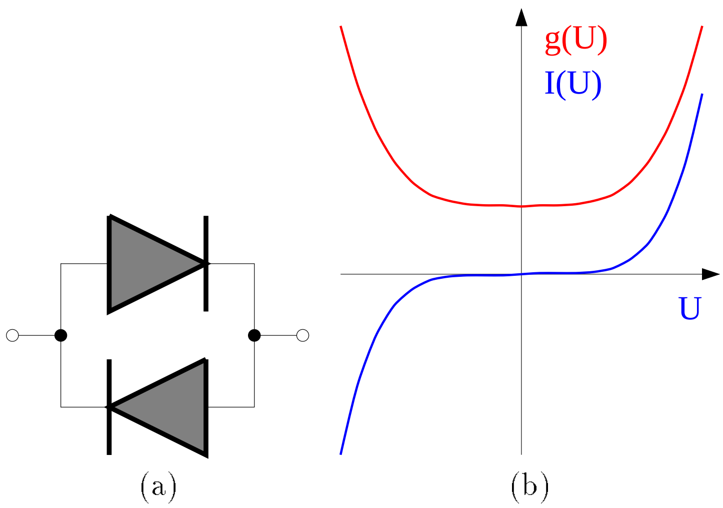

Figure 9: *Anti-parallel pair of diodes (a) and its characteristics (b)*

3.3 Subharmonically pumped mixer

If a diode is pumped with a large single harmonic LO signal $V_{LO}e^{j\omega_p t}$ it can be modelled by small signal parametric conductance $g(t)$ and capacitance $c(t)$, which may be written as Fourier series (19) and (21) respectively. Aplying an additional small signal $I_S e^{j(\omega_s + K\omega_p)t}$ on the diode we achieve mixing signals of the frequencies:

$$\omega_{mix} = |\omega_s + n\omega_p| \tag{42}$$

with n being an integer (see eq. (30)).

Two diodes may be connected together to form an anti-parallel pair (Fig. 9). The characteristic of such an element is then symmetric as shown in the same figure. It has been shown in Sect. 3.1.2 and 3.2.2 that the use of an anti-parallel pair of diodes as a nonlinear element of the mixer results in the large current signal having only odd harmonic components, and the parametric admittance having only even harmonic components. It means that the frequencies of the output signals will be given by (42) with n being an even integer. Fig. 10 shows the large current signal I_n and the parametric conductance G_n in the frequency domain for an anti-parallel pair of diodes pumped with 15GHz LO signal. Choosing the band closest to DC as an output band, the following mixing products are possible:

$$k \cdot 30\text{GHz} \pm IF \rightarrow IF \tag{43}$$

Fig. 10 shows these bands for $0 < IF < 10$GHz. Products with $k = 1$ in (43) are the ones that are used in the project. Therefore the input bands are: 20-30GHz and 30-40GHz and the output band is 0-10GHz (see design specifications in Sect. 2.1). The bands with k higher than 1 are parasitic bands and should be filtered out. However, the complexity of the filter design grows with frequency. The characteristics of the filters (Sect. 4) will be considered only in the band 0-40GHz. Therefore the influence of the higher input bands existence should be tested. It will be performed in Sect. 3.5.4, where we will analyze the circuit numerically.

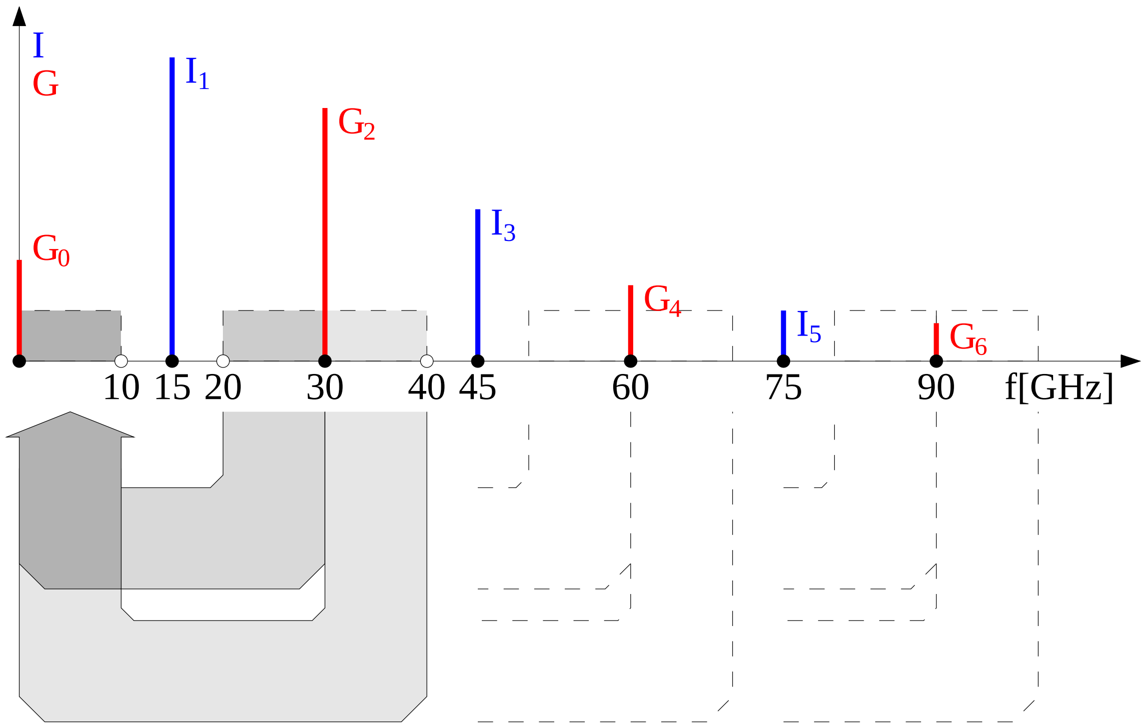

Figure 10: *Anti-parallel pair of diodes pumped with the 15GHz voltage. I – large signal current, G – parametric conductance.*

Frequency (GHz)	1.0 mA Refl. Coeff.		1.5 mA Refl. Coeff.		3.0 mA Refl. Coeff.	
	Mag	Ang	Mag	Ang	Mag	Ang
4	0.752	-7.1	0.607	-7.1	0.511	-7.1
6	0.752	-10.7	0.606	-10.7	0.510	-10.6
8	0.750	-14.3	0.604	-14.3	0.508	-14.2
10	0.749	-18.0	0.602	-17.9	0.506	-17.9
12	0.747	-21.7	0.600	-21.6	0.503	-21.6
14	0.744	-25.5	0.597	-25.4	0.500	-25.4
16	0.742	-29.3	0.593	-29.2	0.496	-29.3
18	0.739	-33.2	0.590	-33.1	0.492	-33.2
20	0.736	-37.2	0.586	-37.2	0.488	-37.3
22	0.732	-41.4	0.581	-41.3	0.483	-41.5
24	0.728	-45.6	0.577	-45.6	0.478	-45.8
26	0.724	-49.9	0.572	-50.0	0.473	-50.3
28	0.720	-54.4	0.567	-54.6	0.467	-55.0
30	0.716	-59.1	0.562	-59.3	0.462	-59.8
32	0.711	-63.9	0.557	-64.2	0.456	-64.9
34	0.707	-68.8	0.552	-69.3	0.451	-70.1
36	0.703	-73.9	0.547	-74.5	0.447	-75.6

Table 1: *RF impedance data for MA40417 diode*

3.4 Diodes

MA40417 beam lead diodes have been chosen for the realization of the mixer. Tab. 1 shows *RF* impedance data for one diode. The diode and its dimensions are shown in Fig. 11. Two diodes are mounted in parallel in the uni-planar circuit[2] (see Fig. 12). The dimensions refer to *Alumina* substrate: $\epsilon_r = 9.9$, $h = 635\mu m$, $t = 10\mu m$. The configuration shown in Fig. 12 introduces large discontinuity to the circuit. For its exact modelling complicated full wave numerical methods should be used[3]. We will model the circuit with the simplest method possible, using ideal transmission lines without considering the influence of discontinuities and dispersion. The discontinuity of the diode connections will not be introduced to the model. Therefore it is important to test the sensitivity of the mixer characteristics to the change of load impedances of the diodes. It will be performed in Sect. 3.5.4, where we will analyze the circuit numerically.

[2]Uni-planar technology will be introduced in Sect. 4.2

[3]such as Finite Elements (FEM), Finite Differences (FD), or Spectral Domain Method

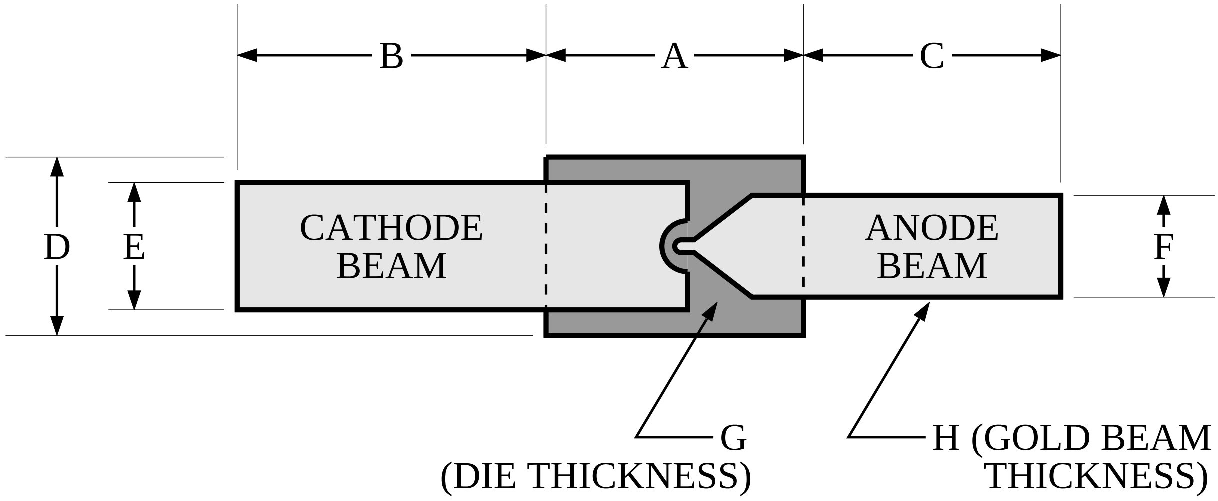

Dimension	Min. [mm]	Max. [mm]
A	0.25	0.30
B	0.30	–
C	0.25	–
D	0.15	0.20
E	0.12	0.15
F	0.10	0.12
G	0.07	0.10
H	0.012 Nominal	

Figure 11: *Chip style 1010 (diode MA40417) and its dimensions*

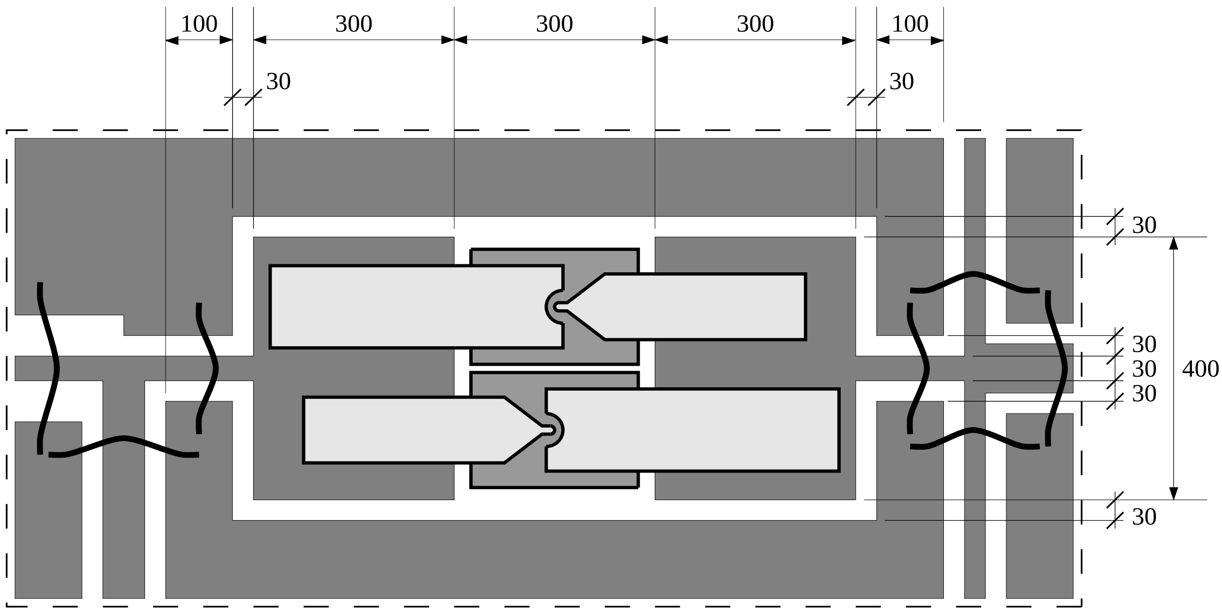

Figure 12: *Montage of the diodes in the uni-planar circuit. All dimensions in μm. Substrate: Alumina, $\epsilon_r = 9.9$, $h = 635\mu m$, $t = 10\mu m$.*

3.5 Numerical nonlinear-linear analysis

3.5.1 Kerr's reflection algorithm

Kerr's reflection algorithm is described in [2, pp. 97–101]. The LO source network and the diode are separated by a section of an ideal transmission line of the characteristic impedance Z_c. The transmission line is assumed to be an integer number of wavelengths long at the fundamental LO frequency, and hence at all its harmonics as well, and therefore does not affect the steady state voltages and currents at diode terminals. It enables incident and reflected waves to be defined, and to spliting the analysis into the linear and nonlinear parts.

Before a reflected wave appears at the input, the transmission line is electrically equivalent to its characteristic impedance Z_c. The incident voltage wave is given by:

$$V_i^{(1)}(t) = \frac{V_{LO} Z_c}{\sqrt{Z_c^2 + |Z_1|^2}} \cos(\omega_p t + \Theta) + \frac{V_B Z_c}{Z_c + Z_0} \tag{44}$$

where

$$\Theta = -\tan^{-1}\left(\frac{\Im(Z_1)}{\Re(Z_1) + Z_c}\right) \tag{45}$$

Z_n	-	Thevenin's impedance of the circuit for n-th LO harmonic,
V_B	-	polarisation source voltage,
V_{LO}	-	harmonic source voltage,

and superscript denotes iteration number.

The incident wave $V_i^{(1)}(t)$ reflects from the diode:

$$V_r^{(1)}(t) = \frac{V_d^{(1)}(t) - I_d^{(1)}(t) Z_c}{2} \tag{46}$$

where

$$V_d^{(1)}(t) = V_i^{(1)}(t - \tau) \tag{47}$$

is the diode incident voltage wave, and $I_d(t)$ is the current response of the diode to $V_d(t)$. The V_r voltage response contains harmonics. The Fast Fourier Transform is used to represent the signal in the frequency domain:

$$V_r^{(1)}(n) = \sum_{m=0}^{M} V_r^{(1)}(mT) e^{jn\omega_p(mT)} \tag{48}$$

where M is the number of points in the discrete representation of the signal.

Every harmonic reflects from the corresponding impedance Z_n at the input with the reflection coefficient Γ_n:

$$\Gamma_n = \frac{Z_n - Z_c}{Z_n + Z_c} \tag{49}$$

and modifies the incident wave:

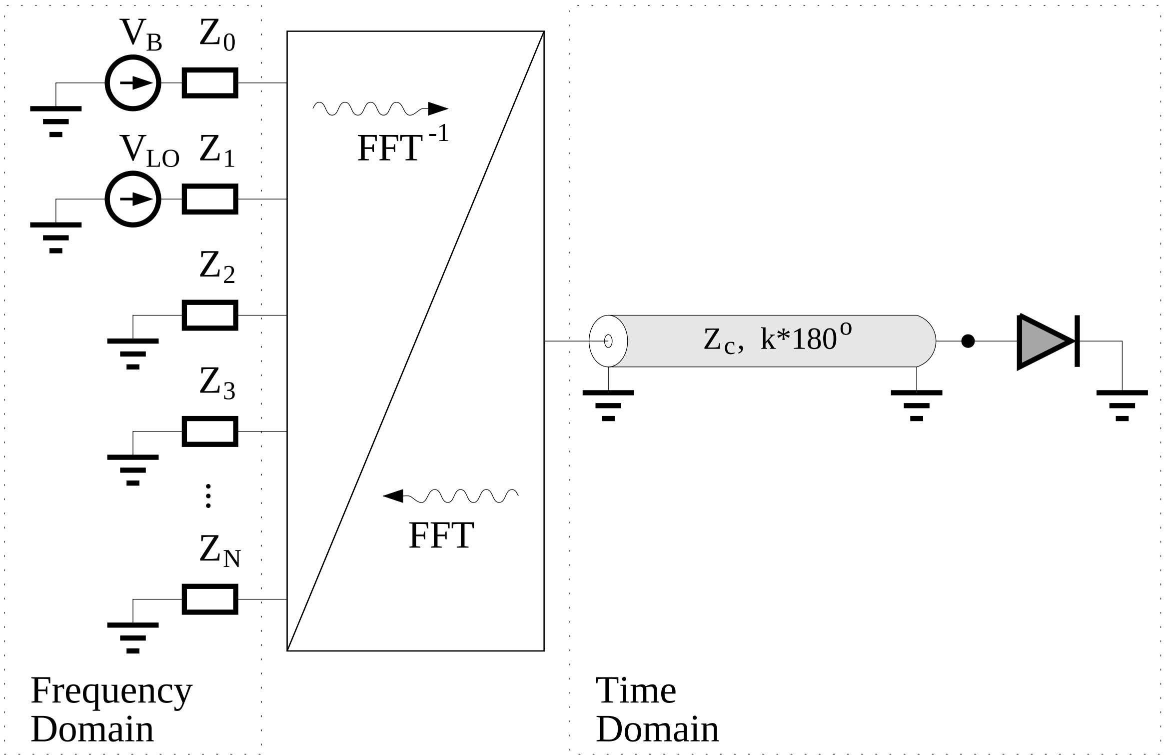

Figure 13: *Kerr's reflection algorithm*

$$V_i^{(2)}(n) = V_i^{(1)}(n) + V_r^{(1)}(n) \cdot \Gamma_n \tag{50}$$

The Inverse Fast Fourier transform is used to represent the new incident wave in the time domain. The new incident wave is used in the next iteration.

This iterative process may have various termination criteria. Usually an error is estimated, i.e.

$$err(k) = \sqrt{\frac{1}{M}\sum_{m=0}^{M}\left[(V_d^{(k-1)}(mT))^2 + (V_d^{(k)}(mT))^2\right]} \tag{51}$$

with the termination criterion:

$$err(k) \leq err_{MAX} \tag{52}$$

The transmission line's characteristic impedance Z_c may be chosen arbitrarily; this value has no influence on the solution of the problem. However, it may have an influence on the iteration convergence speed. The algorithm has been used in the project with 50Ω transmission line.

The idea of the Kerr's reflection algorithm is shown in Fig. 13.

3.5.2 Numerical modelling of parametric circuits

The most important parameter of a mixer is conversion loss (L_c). It is defined as the ratio of small signal source available power to the power delivered to the load at the output mixing frequency:

$$L_{cK} = 10\lg\frac{P_{S(0)}}{P_{S(K)}} \tag{53}$$

where indices in P_S and L_c denote the bands (n in eq. (42)). In this project the output band is the one closest to DC (n=0), and two input bands have indices $n = K = \pm 2$. The available source power (Norton's model in Fig. 5) is given by:

$$P_{S(K)} = \frac{|I_{S(K)}|^2}{8\Re[Y(\omega_s + K\omega_p)]} \tag{54}$$

We will calculate the power delivered to the load at the output mixing frequency ($P_{S(0)}$).

The unknown complex voltage magnitudes V_{Sn} in (29) should be calculated. Equation (29) is an infinite series, and in a general case its exact solution is impossible. In the numerical modelling the equation is truncated at $m = \pm N$ and $n = \pm N$:

$$\begin{aligned} I_{S(K)}e^{j(\omega_s+K\omega_p)t} &= \sum_{m=-N}^{N} Y(\omega_s + m\omega_p)V_{Sm}e^{jk(\omega_s+m\omega_p)t} + \\ & \sum_{m=-N}^{N}\sum_{n=-N}^{N} Y_{mn}V_{Sn}e^{jk[\omega_s+(m+n)\omega_p]t} \end{aligned} \tag{55}$$

Equation (55) may by written in a matrix form:

$$\begin{bmatrix} 0 \\ \vdots \\ 0 \\ I_{S(K)} \\ 0 \\ \vdots \\ 0 \end{bmatrix} = \left(\begin{bmatrix} Y(\omega_s - N\omega_p) & 0 & \cdots & & 0 \\ 0 & & \ddots & & \vdots \\ \vdots & & & \ddots & 0 \\ 0 & & \cdots & 0 & Y(\omega_s + N\omega_p) \end{bmatrix} + \right.$$
$$\left. \begin{bmatrix} Y_{0,-N} & Y_{-1,-N} & Y_{-2,-N} & \cdots & Y_{-2N,-N} \\ Y_{1,-N+1} & Y_{0,-N+1} & Y_{-1,-N+1} & \cdots & Y_{-2N+1,-N+1} \\ \vdots & \vdots & \vdots & \ddots & \vdots \\ Y_{2N,N} & Y_{2N-1,N} & Y_{2N-2,N} & \cdots & Y_{0,N} \end{bmatrix} \right) \begin{bmatrix} V_{S(-N)} \\ V_{S(-N+1)} \\ \vdots \\ V_{S(N)} \end{bmatrix} \tag{56}$$

or in a more compact form:

$$\underline{I_S} = \underline{\underline{Y_S}} \cdot \underline{V_S} \tag{57}$$

By elimination of variables, (57) may be converted to:

$$\begin{bmatrix} 0 \\ I_{S(K)} \end{bmatrix} = \begin{bmatrix} Y_{S(0,0)} & Y_{S(0,K)} \\ Y_{S(K,0)} & Y_{S(K,K)} \end{bmatrix} \begin{bmatrix} V_{S(0)} \\ V_{S(K)} \end{bmatrix} \tag{58}$$

relating the RF and IF port voltages and the source RF current. Equation (58) is a set of 2 linear equations with 2 unknowns, and can easily be solved.

The output IF power may then be calculated from:

$$P_{S(0)} = \frac{1}{8}|V_{S(0)}|^2 \cdot \Re[Y(\omega_s)] \tag{59}$$

Putting (54) and (59) into (53) and considering (22) and (23) gives an expression for conversion loss:

$$\begin{aligned} L_{cK} &= 10\lg \frac{|I_{S(K)}|^2}{|V_{S(0)}|^2 \cdot \Re[Y(\omega_s)] \cdot \Re[Y(\omega_s + K\omega_p)]} = \\ & 10\lg \frac{|V_{S(K)}|^2}{|V_{S(0)}|^2} \cdot \frac{\Re[Z(\omega_s)]}{\Re[Z(\omega_s + K\omega_p)]} \end{aligned} \tag{60}$$

3.5.3 Software description

The computer program *DIODEMX* (listed and described in [2, App. A]) has been used for nonlinear-linear analysis of the mixer[4]. *DIODEMX* is written in *PASCAL* and consists of two parts:

- Large-signal analysis, which is an implementation of the Kerr's algorithm (Sect. 3.5.1)
- Small-signal analysis, based on the data from previous point (Sect. 3.5.2)

The input of the program is a file with the following format ([2, p. 315]):

DIODE	I_0 n C_{j0} Φ γ R_s $temp$
VOLTS	V_{LO} V_{bias}
POWER	P_{LO}
FREQS	*LOfreq IFfreq*
MISCL	Z_c tol
ZSIG1	Z_{s-4} Z_{s-3} Z_{s-2} Z_{s-1}
ZSIG2	Z_{s0} Z_{s1} Z_{s2} Z_{s3} Z_{s4}
ZELO1	Z_0 Z_1 Z_2 Z_3
ZELO2	Z_4 Z_5 Z_6 Z_7 Z_8

DIODE lists the diode parameters:

I_0	– Current parameter for the I/V characteristic [A];
n	– Ideality factor;
C_{j0}	– Zero-voltage junction capacitance [F];
Φ	– Junction built-in potential [V];
γ	– Exponent for the capacitance characteristic (0.5);
R_s	– Series resistance [Ω];
$temp$	– Temperature [K].

VOLTS lists *LO* and *bias* voltages:

V_{LO}	– The *LO* source open-circuit peak value ($P_{LO} = V_{LO}^2/8\Re[Z_s(\omega_p)]$);
V_{bias}	– The *DC* bias voltage.

POWER[5] – if it exists the value of V_{LO} is ignored:

P_{LO}	– The *LO* source available power.

FREQS lists *LO* and *IF* frequencies [Hz]:

[4]The program has been slightly modified to allow simple optimization

[5]This entry doesn't exist in the original program.

LOfreq	– The applied *LO* frequency;
IFfreq	– The mixing frequency closest to *DC*.

MISCL list miscellaneous parameters:

Z_c	– The characteristic impedance of the fictitious transmission line in the large-signal Kerr's algorithm (Sect. 3.5.1);
tol	– The value of the error function at which the large-signal algorithm will terminate.

ZSIG1 and **ZSIG2** list the small-signal embedding impedances:

Z_{sn}	– The embedding impedance at ω_n in real and imaginary form. The real part is first, then the imaginary.

ZELO1 and **ZELO2** list the *LO* harmonic embedding impedances:

Z_n	– The embedding impedance of the *LO* harmonic at $n\omega_p$. Zero must be entered for the imaginary part of Z_0. Impedances are in real and imaginary form with the real part first.

Fig. 14 shows a sample input file for the program.

After reading an input file, *DIODEMX* runs the Kerr's reflection algorithm iterative procedure. It terminates if the error function (eq. (51)) drops below *tol* on the MISCL line, or changes less than the internal tolerance since the last iteration.

For the small-signal analysis, the user is prompted for the indices of the input and output frequency; i.e., the values of n for the frequencies $\omega_0 + n\omega_p$. In this project, these are 2 and 0, and -2 and 0.

```
DIODE  7.0e-14  1.15  0.07e-12  0.86  0.5  8.0  295.0
VOLTS  0.0  0.0
POWER  2e-3
FREQS  15e9  5e9
MISCL  50.0  0.0005
ZSIG1    0.00  0.00    0.00  0.00  100.00  0.00    0.00 0.00
ZSIG2  100.00  0.00    0.00  0.00  100.00  0.00    0.00 0.00    0.00 0.00
ZELO1    0.00  0.00  100.00  0.00    0.00  0.00    0.00 0.00
ZELO2    0.00  0.00    0.00  0.00    0.00  0.00    0.00 0.00    0.00 0.00
```

Figure 14: *Sample input file for DIODEMX program. Analysis of an anti-parallel pair of diodes using an equivalent one diode model* ($Z_{2n} = Z_{s2n+1} = 0$, $Z_{2n+1} = 2Z'_{2n+1}$, $Z_{s2n} = 2Z'_{s2n}$ *(n=0,1,2,...)*, $P_{LO} = \frac{1}{2}P'_{LO}$*; where primed are the parameters of the circuit with an anti-parallel pair of diodes (see. Sect. 3.5.2)).* $P'_{LO} = 4mW$, $Z'_1 = Z'_{s0} = Z'_{s-2} = Z'_{s2} = 50\Omega$, $Z'_{2n+1} = 0$ *for* $n \geq 1$, $Z'_{2n} = 0$ *for* $n > 1$ *and* IFfreq = *5GHz.*

3.5.4 Results of nonlinear-linear analysis

In the numerical nonlinear-linear analysis of the mixer, the computer programme *DIODEMX* introduced in Sect. 3.5.3 has been used. The simulations have been performed for an anti-parallel pair of diodes with parameters typical for the K band. The following is the list of a diode parameters:

$$\begin{aligned} I_0 &= 7 \cdot 10^{-14}\mathrm{A} \\ n &= 1.15 \\ C_{j0} &= 0.07\mathrm{pF} \\ \Phi &= 0.86\mathrm{V} \\ \gamma &= 0.5 \\ R_s &= 8\Omega \\ temp &= 295\mathrm{K} \end{aligned}$$

LO **power.** Tab. 2 presents conversion losses and load impedances of the diodes as a function of the LO power. It was assumed that the diodes were matched at the LO (15GHz) frequency (large signal model):

$$Z'_1 = Z'^*_d(15\mathrm{GHz}) \tag{61}$$

and in input and output bands (small signal model):

$$Z'_{S\pm2} = Z'^*_d(30\mathrm{GHz} \pm IF) \tag{62}$$

$$Z'_{S0} = Z'^*_d(IF) \tag{63}$$

where $Z'_d(f)$ denotes input impedance of the diodes, * denotes complex conjugation, and IF is the output frequency: $0 < IF < 10\mathrm{GHz}$.

The Thevenin's impedances of the circuit were set to 0 (shunts) at higher harmonic frequencies ($Z'_{2n'+1}$, $n' \geq 1$) and in the higher order (parasitic) input bands ($Z'_{S\pm2n'}$, $n' > 1$) Realization of shunts in the higher bands using simple design technique introduced in Sect. 4 is not possible for the considered substrates. Therefore, the sensitivity of the circuit to the change of these impedances will be tested.

Tab. 3 presents conversion losses as a function of the LO power when impedances Z'_1, $Z'_{S\pm2}$ and Z'_{S0} are set to 50Ω. Like in the last case, the impedances in higher bands are set to 0.

Tab. 3 is of more practical importance than Tab. 2. It is easier to design filters in 50Ω system than wide-band matching circuits, which should be realized to match the diodes and satisfy the assumptions from Tab. 2.

LO_{eff} in Tab. 3 is the local oscillator efficiency describing the LO port matching. Three L_C factors have been considered:

$$\begin{array}{ll} L_{C-2}(IF = 10\mathrm{GHz}) & \text{for } 20\mathrm{GHz} \to 10\mathrm{GHz} \text{ product} \\ L_{C\pm2}(IF = 0) & \text{for } 30\mathrm{GHz} \to 0 \text{ product} \\ L_{C+2}(IF = 10\mathrm{GHz}) & \text{for } 40\mathrm{GHz} \to 10\mathrm{GHz} \text{ product} \end{array}$$

The $L_C(IF)$ characteristic should be flat. Therefore these values should be comparable. The differences ΔL_c decrease with the increasing LO power.

Small signal modelling. Next set of tables presents results of the small signal analysis. The diodes are pumped with a 4mW *LO* signal. This value has been chosen arbitrarily and is not the optimal one. The *LO* power should be verified by an experiment.

Tab. 4 presents conversion losses and load impedances of the diodes as a function of the *IF* frequency. It was assumed that the diodes were matched at *LO* frequency ((61)) and in input ((62)) and output ((63)) bands. Since wide-band matching circuit design is very difficult[6] Tab. 4 is of no practical importance.

Tab. 5 presents conversion losses as a function of the *IF* frequency for the case when the diodes are matched at *LO* frequency[7] ((61)) and terminated by the 50Ω impedances in input and output bands.

Tab. 6 presents the same data for the case when the diodes are terminated by the 50Ω impedance at *LO* frequency. The data from Tab. 5 and 6 do not differ significantly. Therefore all the filters will be designed in 50Ω system.

The minimum and maximum values of the conversion losses and the differences between them are:

- Input band: 20–30GHz
  - $L_{Cmin} = L_C(20\text{GHz}) = 7.4\text{dB}$
  - $L_{Cmax} = L_C(30\text{GHz}) = 7.9\text{dB}$
  - $\Delta L_C = 0.5$
- Input band: 30–40GHz
  - $L_{Cmin} = L_C(30\text{GHz}) = 7.9\text{dB}$
  - $L_{Cmax} = L_C(40\text{GHz}) = 9.3\text{dB}$
  - $\Delta L_C = 1.4$

ΔL_C should be minimized. It may be optimized by experimentally choosing the optimal *LO* power. If it does not give satisfactory results, correctors may be designed, for instance as external circuits (one per input band) connected to the output mixer port.

Sensitivity to the change of impedances. In the simulations presented above, it was assumed that the diodes were terminated by shunts at higher harmonic frequencies and in higher order input bands. In the linear part of the project (Sect. 4) very simple filter models will be used. We shall not consider the influence of discontinuities and dispersion in transmission lines. Characteristics of the filters will be only considered for the band 0–40GHz. Therefore, load impedances of the diodes are unknown at higher frequencies and sensitivity of conversion losses to the change of these impedances will be tested. It has to be noted that it will be just an estimation of the actual sensitivity. To have more exact results, software more powerful than *DIODEMX* should be used.

[6] In practice, considering the impedances which should be realized, even impossible in uni-planar technology on substrates listed in design specifications (Sect. 2.1).

[7] Since *LO* signal has constant frequency it is easy to construct appropriate matching circuit.

Impedances Z'_1, $Z'_{S\pm2}$ and Z_{S0} are set to 50Ω. Impedances in higher bands are set to 0, except for the one which is tested.

Tab. 7 presents sensitivity of the conversion losses to the change of $Z'_3 = Z'(45\text{GHz})$ impedance. Z'_3 takes various values from the positive complex half-plane $\Re(Z'_3) \geq 0$. L_c and ΔL_c factors are tested. In the worst cases $\Delta L_{c-2max} = 0.7\text{dB}$ and $\Delta L_{c2max} = 2.0\text{dB}$.

Tab. 8 presents sensitivity of the conversion losses to the change of $Z_{s4} = Z'(60\text{GHz}+IF)$ and $Z_{s-4} = Z'(60\text{GHz-}IF)$. Z_{s4} and Z_{s-4} takes the same values from positive complex half-plane $\Re(Z'_{s\pm4}) \geq 0$. In the worst case $\Delta L_{c-2max} = 0.8\text{dB}$. The change of ΔL_{c2} is not significant ($\Delta L_{c2max} = 1.4\text{dB}$).

As we will see in Sect. 4, the anti-parallel pair of diodes is connected in series between low pass and band pass filters. The filters have opposite characteristics, i.e. the low pass filter passes and the band pass filter reflects all the signal in the band 0–15GHz, while in the band 20–40GHz the band pass filter passes all the signal and the low pass filter reflects it. Since we assumed 50Ω terminations of the diodes, the filters should approximate a shunt in their stop bands. This condition splits into two parts:

- The magnitude of the reflection coefficients should be approximately 1 (or 0dB)
- The phase of reflection coefficients should approximately be equal to 180^o

The first condition is easy to satisfy, and it will be a condition for optimization of the filters. The second one, however, is impossible to satisfy in all the bands (0–15GHz and 20–40GHz) and therefore the load impedances will have nonzero imaginary parts. Their influence on the conversion losses will be tested.

Tab. 9 shows the influence of the low pass filters impedance in the band 20–40GHz on the conversion losses. The low pass filter (F0-15) will be introduced in Sect. 4.4. Fig. 33(b) shows the reflection coefficient of its idealized model after optimization. At 30GHz, the reflection coefficient is an exact shunt. The magnitude characteristic of the reflection is symmetric and its phase characteristic is anti-symmetric around 30GHz. The filter is a conductive reactance in the band 20–30GHz, and an inductive reactance in the band 30–40GHz. Therefore the impedances Z'_{s-2} and Z'_{s2} may be expressed by symmetric equations:

$$Z'_{s-2} = 50\Omega - j\alpha \tag{64}$$

$$Z'_{s2} = 50\Omega + j\alpha \tag{65}$$

with α being a positive real value. For $\alpha = 50\Omega$ the reflection phase changes by 90^o. Tab. 9 shows that the filter has the largest effect in the lower input band (20–30GHz), where, for $IF = 10\text{GHz}$, conversion losses increase from 7.4dB to 9.4dB, i.e. by 2dB. Also, the difference between the L_C peak values increases to $\Delta L_C = 1.5\text{dB}$. In the higher input band (30–40GHz), conversion losses increase by about 0.5dB and ΔL_C increases to 1.8dB.

Tab. 10 shows the influence of the band pass filters impedance on the conversion losses for the band 0–10GHz. The band pass filter (F20-40) will be introduced in Sect. 4.5. Fig. 37(b) shows the reflection coefficient of its idealized model after optimization. The reflection coefficient is a shunt at DC and behaves like a growing inductance with growing frequency. Therefore the impedance Z'_{s0} may be expressed by:

$$Z'_{s0} = 50\Omega + j\beta \tag{66}$$

			$IF = 0$			
P'_{LO}	$Z'_1[\Omega]$		$Z'_{s\pm2}[\Omega]$		$L_{c\pm2}$	Z'_{s0}
[mW]	$\Re$	$\Im$	$\Re$	$\Im$	[dB]	$[\Omega]$
0.5	9.54	69.43	9.84	33.33	6.65	235.64
0.7	12.54	68.57	12.21	32.38	6.31	179.17
1.0	16.27	67.17	14.78	30.82	6.16	141.01
1.5	21.94	64.07	18.00	27.77	6.19	105.55
2.0	26.21	60.78	19.79	24.98	6.33	86.85
3.0	32.26	53.64	21.34	20.42	6.67	65.64
4.0	35.56	47.19	21.56	17.23	6.99	54.11
5.0	37.21	41.47	21.33	14.88	7.30	46.48
6.0	37.75	36.54	20.91	13.05	7.59	40.97
7.0	37.75	32.60	20.45	11.70	7.83	37.13
8.0	37.35	29.20	20.01	10.62	8.06	34.21
9.0	36.79	26.38	19.58	9.74	8.26	31.90
10.0	36.12	24.01	19.18	9.01	8.45	30.04

$Z'_1 = Z'^*_d(\omega_0)$, $Z'_{s\pm2} = Z'^*_{ds}(\omega_0 \pm \omega_s)$, $Z'_{s0} = Z'^*_{ds}(\omega_s)$

Table 2: *Large and small signal analysis results. Conversion losses and load impedances of the diodes as functions of the LO power. Diodes matched at LO (15GHz (Z'_1)) frequency and in input (30GHz ± IF ($Z'_{s\pm2}$)) and output (IF (Z'_{s0})) bands.*

with β being a positive real value. For $\beta = 50\Omega$ the reflection phase changes by 90^o. Tab. 9 shows that the filter has no significant influence on the conversion losses.

		$IF = 10$GHz				
			$IF = 0$			
P'_{LO} [mW]	LO_{eff} [%]	L_{c-2} [dB]	L_{c-2} [dB]	L_{c2} [dB]	ΔL_{c-2} [dB]	ΔL_{c-2} [dB]
2	0.18	11.55	12.93	15.57	1.38	2.64
3	0.45	7.35	8.19	9.95	0.84	1.76
4	0.59	7.37	7.86	9.25	0.49	1.39
5	0.70	7.66	7.98	9.06	0.32	1.08
6	0.77	8.06	8.22	9.22	0.16	1.00
7	0.82	8.41	8.50	9.39	0.09	0.89
8	0.85	8.73	8.78	9.59	0.05	0.81
9	0.87	9.02	9.05	9.80	0.03	0.75
10	0.89	9.30	9.30	10.00	0.00	0.70
$Z'_1 = Z'_{s0} = Z'_{s-2} = Z'_{s2} = 50\Omega$						

Table 3: *Large and small signal analysis results. Conversion losses as a function of the LO power. Diodes terminated by* 50Ω *impedances at LO (15GHz (Z'_1)) frequency and in input (30GHz $\pm$ IF ($Z'_{s\pm2}$)) and output (IF (Z'_{s0})) bands.*

IF	$Z'_{s-2}[\Omega]$		$Z'_{s2}[\Omega]$		L_{c-2}	L_{c2}	$Z'_{s0}[\Omega]$	
[GHz]	$\Re$	$\Im$	$\Re$	$\Im$	[dB]	[dB]	$\Re$	$\Im$
0	21.57	17.23	21.57	17.23	6.99	6.99	54.11	0.00
1	22.20	17.20	20.95	17.23	6.97	7.02	53.97	2.62
2	22.87	17.14	20.36	17.21	6.95	7.05	53.54	5.19
3	23.55	17.05	19.78	17.17	6.93	7.08	52.84	7.67
4	24.24	16.91	19.22	17.10	6.91	7.12	51.91	10.03
5	24.95	16.73	18.70	17.02	6.90	7.16	50.77	12.21
6	25.67	16.52	18.19	16.91	6.89	7.20	49.43	14.22
7	26.41	16.25	17.70	16.80	6.88	7.24	47.96	16.04
8	27.15	15.94	17.23	16.67	6.88	7.29	46.38	17.64
9	27.90	15.58	16.79	16.54	6.88	7.34	44.73	19.03
10	28.65	15.16	16.37	16.40	6.88	7.39	43.03	20.22
$P'_{LO} = 4mW$ $Z'_1 = Z'^{*}_{d}(\omega_0) = 36 + j47,\ Z'_{s\pm2} = Z'^{*}_{ds}(\omega_0 \pm \omega_s),\ Z'_{s0} = Z'^{*}_{ds}(\omega_s)$								

Table 4: *Small signal analysis results. Conversion losses and load impedances of the diodes as functions of mixing frequency. Diodes matched at LO (15GHz (Z'_1)) frequency and in input (30GHz $\pm$ IF ($Z'_{s\pm2}$)) and output (IF (Z'_{s0})) bands.*

IF [GHz]	L_{c-2} [dB]	L_{c2} [dB]
0	8.05	8.05
5	7.83	8.49
10	7.83	9.09

$Z'_1 = Z^*_d(\omega_0) = 36 + j47\Omega$
$Z'_{s0} = Z'_{s-2} = Z'_{s2} = 50\Omega$
$P'_{LO} = 4mW$

Table 5: *Small signal analysis results. Conversion losses as a function of mixing frequency. Diodes matched at LO (15GHz (Z'_1)) frequency and terminated by* 50Ω *in input (30GHz* $\pm$ *IF ($Z'_{s\pm2}$)) and output (IF (Z'_{s0})) bands.*

IF [GHz]	L_{c-2} [dB]	L_{c2} [dB]
0	7.86	7.86
1	7.77	7.96
2	7.69	8.07
3	7.62	8.19
4	7.55	8.32
5	7.50	8.45
6	7.46	8.60
7	7.42	8.75
8	7.40	8.91
9	7.38	9.08
10	7.37	9.25

$Z'_1 = Z'_{s0} = Z'_{s-2} = Z'_{s2} = 50\Omega$
$P'_{LO} = 4\mathrm{mW}$

Table 6: *Small signal analysis results. Conversion losses as a function of mixing frequency. Diodes terminated by* 50Ω *at LO (15GHz (Z'_1)) frequency and in input (30GHz* $\pm$ *IF ($Z'_{s\pm2}$)) and output (IF (Z'_{s0})) bands.*

	$IF = 10\text{GHz}$				
		$IF = 0$			
Z'_3 [Ω]	L_{c-2} [dB]	$L_{c\pm2}$ [dB]	L_{c2} [dB]	ΔL_{c-2} [dB]	ΔL_{c2} [dB]
0	7.37	7.86	9.25	0.49	1.39
50	7.77	8.31	9.10	0.54	0.79
$j50$	8.63	9.30	10.83	0.67	1.53
$-j50$	7.37	7.97	9.49	0.60	1.52
$50+j50$	8.01	8.59	10.05	0.58	2.04
$50-j50$	7.65	8.18	9.62	0.53	1.44
∞	7.54	8.12	9.64	0.58	1.52

Table 7: *Influence of load impedance of the diodes at 45GHz (Z'_3) on the conversion losses of the mixer.*

	$IF = 10\text{GHz}$				
		$IF = 0$			
Z'_{s-4}, Z'_{s4} [Ω]	L_{c-2} [dB]	$L_{c\pm2}$ [dB]	L_{c2} [dB]	ΔL_{c-2} [dB]	ΔL_{c2} [dB]
0	7.37	7.86	9.25	0.49	1.39
50	8.03	8.71	10.13	0.68	1.42
$j50$	8.36	9.16	10.54	0.80	1.38
$-j50$	8.29	8.75	10.02	0.46	1.27
$50-j50$	8.17	8.89	10.30	0.72	1.41
$50+j50$	8.20	8.76	10.18	0.56	1.42
∞	8.44	8.97	10.24	0.53	1.27

Table 8: *Influence of load impedance of the diodes at 60GHz ± IF (Z'_3) on the conversion losses of the mixer.*

	$IF = 10$GHz				
		$IF = 0$			
α [Ω]	L_{c-2} [dB]	$L_{c\pm2}$ [dB]	L_{c2} [dB]	ΔL_{c-2} [dB]	ΔL_{c2} [dB]
0	7.37	7.86	9.25	0.49	1.39
50	9.38	–	9.70	(-)1.52	1.84
500	23.28	–	26.01	(-)15.42	18.15
		$Z'_{s-2} = 50\Omega - j\alpha$, $Z'_{s2} = 50\Omega + j\alpha$			

Table 9: *Influence of F0-15 low pass filter reactance in the band 20-40GHz (see Sect. 4.4 and Fig. 33(b)) on the conversion losses of the mixer.*

	$IF = 10$GHz				
		$IF = 0$			
β [Ω]	L_{c-2} [dB]	$L_{c\pm2}$ [dB]	L_{c2} [dB]	ΔL_{c-2} [dB]	ΔL_{c2} [dB]
0	7.37	7.86	9.25	0.49	1.39
50	7.34	–	9.22	0.52	1.36
75	8.11	–	9.98	(-)0.25	2.12
500	23.28	–	26.01	(-)15.42	18.15
		$Z'_0 = 50\Omega + j\beta$			

Table 10: *Influence of F20-40 band pass filter reactance in the band 0-10GHz (see Sect. 4.5 and Fig. 37(b)) on the conversion losses of the mixer.*

4 Filters

The nonlinear-linear analysis presented in Sect. 3 gives conditions for the linear part of the project. In this section we focus on the filters design. Sect. 4.1 introduces a block model of the mixer with conditions which the filters should satisfy. The filters will be realized in uni-planar technology, introduced in Sect. 4.2, using distributed elements presented in Sect. 4.3. Sect. 4.4, 4.5 and 4.6 present modelling, realization and results of measurements of the filters. The final circuit with all the components together is presented in Sect. 4.7. This part of the project has been performed in *Ecole Nationale Supérieure des Télécommunications de Bretagne*, in Brest. The *MDS-HP* software has been used in the modelling of the filters.

4.1 Block model of the mixer

Fig. 15 shows the block model of the mixer. The mixer has three ports:

LO	–	local oscillator port signal with constant frequency 15GHz
IN	–	input port signal from two input bands: 20-30GHz ($G_{-2} \to G_0$), 30-40GHz ($G_2 \to G_0$)
OUT	–	output port signal from the band 0-10GHz

Tab. 11 shows the pass-bands and stop-bands of the filters.

Filter	Pass-band	Stop-band(s)
F20-40	20–40GHz	0–15GHz
F0-10	0–10GHz	15GHz and 20–40GHz
F15	15GHz	0–10GHz and 20–40GHz

Table 11: Pass-bands and stop-bands of the filters

As a compromise between the needs and possibilities of the technology the minimal attenuation in the stop-bands has been set to 20dB, and maximal attenuation in the pass-bands has been set to 0.25dB.

In the nonlinear-linear analysis of the mixer (Sect. 3) we saw that in order to achieve optimal energy conditions, the following additional conditions should be satisfied:

- The reflection coefficient of the filters on the right side of the diodes should approximate a shunt in the pass-band of the filter F20-40 (20–40GHz) (see Fig. 16). This condition would be difficult to achieve in the circuit from Fig. 15, since it should be satisfied in the plane of interconnection between two filters and the diodes. Therefore, to make this configuration simpler, an additional F0-15 low pass filter has been used between the diodes and the filters F0-10 and F15 (see Fig. 17). The additional filter should not perturb the transmission characteristics of these two filters. It is used to satisfy the condition on the reflection coefficient in the stop-band. The F0-15 filter should satisfy the following conditions:

Pass band. The filter should pass the signals from the pass-bands of the filters F0-10 (0–10GHz) and F15 (15GHz). It was optimized as a low pass filter with the pass-band: **0–15GHz**.

Stop band: 20–40GHz. The reflection coefficient of the filter should approximate a shunt in this band.

- The reflection coefficient of the filter F20-40 on the side of the diodes should approximate a shunt in the pass-bands of the filters F0-10 (0–10GHz) and F15 (15GHz) (see Fig. 18). This condition is the most important in the output band 0–10GHz. At the local oscillator frequency it hasn't such importance since it is just single frequency. It is easy to match the circuit at one frequency using simple configuration (i.e. a cascade transmission line of an appropriate length and a stub of appropriate parameters (length, impedance)). The matching circuit has not been designed, however. It can be realized as an independent circuit with a possibility of tuning. As shown in the nonlinear-linear analysis (Sect. 3.5.4), the load impedance of diodes (50Ω) is not the optimal one at LO frequency. Therefore a need of the use of such an external circuit should be verified by experiment.

Tab. 11 shows the pass-bands and stop-bands of the modified circuit filters.

Filter	Pass-band	Stop-band
F20-40	20–40GHz	0–15GHz
F0-15	0–15GHz	20–40GHz
F0-10	0–10GHz	15GHz
F15	15GHz	0–10GHz

Table 12: Pass-bands and stop-bands of the filters

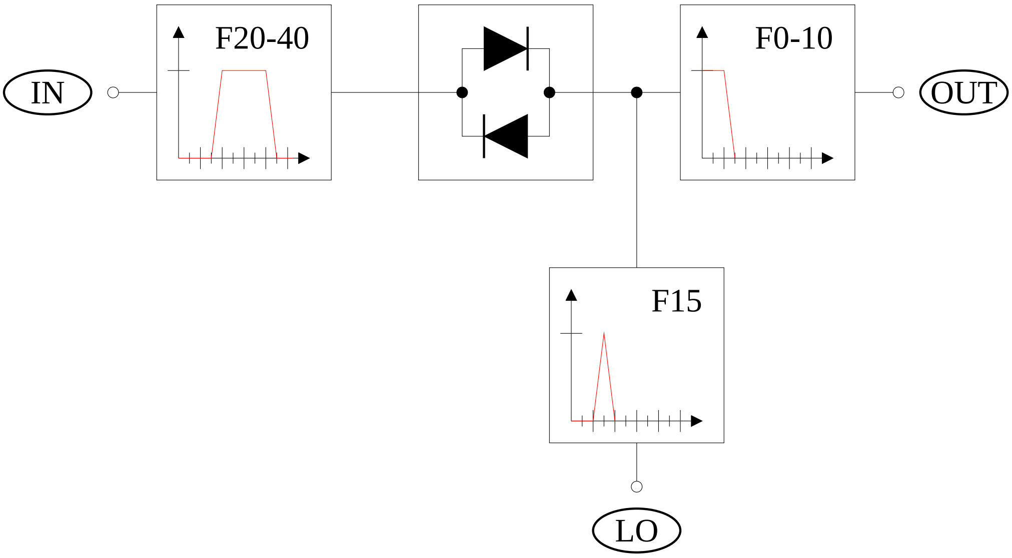

Figure 15: *Block model of the mixer*

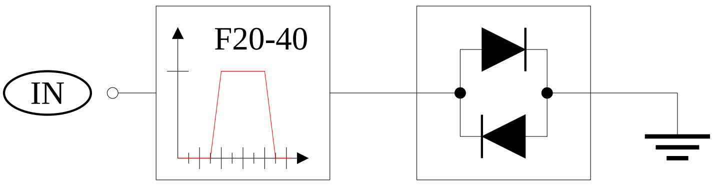

Figure 16: *Block model of the mixer in the frequency band 20-40GHz. The filters on the right side should be a shunt in the plane of the connection with the diodes.*

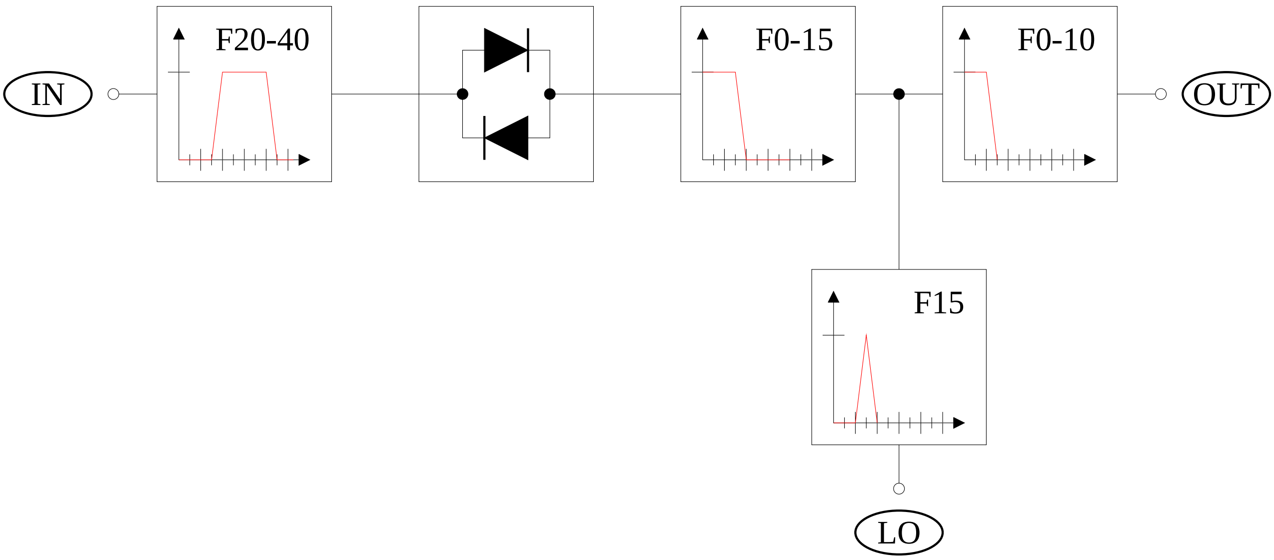

Figure 17: *Modified block model of the mixer*

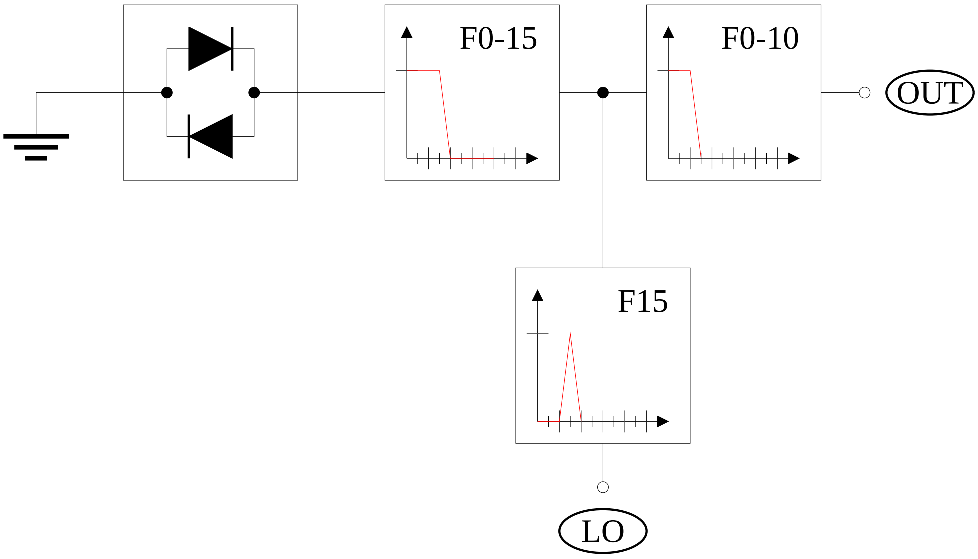

Figure 18: *Block model of the mixer in the frequency band 0-15GHz. The filter F20-40 should be a shunt in the plane of the connection with the diodes.*

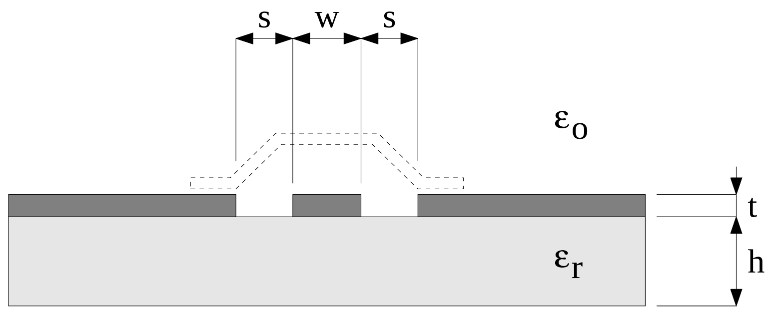

Figure 19: *Coplanar line*

4.2 Uni-planar technology

In the uni-planar technology a transmission line is realized on a substrate consisting of one dielectric and one metal plane, as a single slot (slot-line – Sect. 4.2.3) or two coupled slots (coplanar line – Sect. 4.2.2). The properties of such transmission lines depend on the substrate. Substrates considered in the project are presented in Sect. 4.2.1.

4.2.1 Substrates

The substrates which have been considered in the project are presented in Tab. 13.

Material	ϵ_r	$h[\mu m]$	$t[\mu m]$	$w_{min}[\mu m]$	$s_{min}[\mu m]$
EPSILAM	10.2	635	20	50	50
Alumina	9.9	635	10	30	30
DUROID	2.2	254	20	50	50

Table 13: Substrates considered in the project

The parameters which appear in the table are:

ϵ_r — relative dielectric permitivity
h — dielectric plane thickness
t — metal plane thickness
w_{min} — minimal strip width
s_{min} — minimal slot width

4.2.2 Coplanar line

Fig. 19 shows a cross-section of a coplanar line. Since there are three metal planes in the coplanar line, it may propagate two modes without cutoff frequency, namely the even and the odd mode. The even mode has much better properties for the filter design, i.e. the characteristic impedance is better defined. Therefore we work only with the even mode and conductive bridges between two ground-planes are used to eliminate the odd mode. A bridge is shown in Fig. 19 with the dashed line.

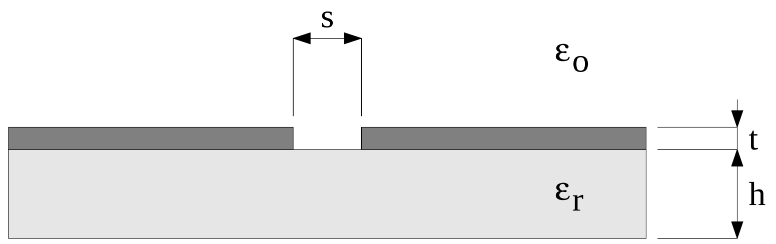

Figure 20: *Slot line*

Since discontinuities are not considered in this project they should be minimized. It is achieved by the minimization of their transverse dimensions with respect to the wavelength. This condition will be tested at the highest frequency considered in the filter design – 40GHz. The ratio of the transverse line dimensions ($w + 2s$) to the wavelength at 40GHz versus the strip and slot widths is shown in the following figures and tables together with the characteristic impedance:

Fig. 21 and Tab. 14	for *EPSILAM*
Fig. 21 and Tab. 15	for *Alumina*
Fig. 22	for *DUROID*

The optimal impedance for the *EPSILAM* and *Alumina* substrates is about 62Ω (i.e. impedance obtained with the smallest dimensions of s and w). The range 50–75Ω has been chosen for both substrates. In this case $\frac{w+2s}{\lambda(40GHz)}$ is 0.079 (*EPSILAM*) and 0.044 (*Alumina*). This range has been chosen arbitrarily. The results of the measurements of the filters will show validity of such an aproach. In the case of *Alumina* substrate discontinuities are much smaller, since smaller strip and slot widths can be realized. *DUROID* cannot be used in the coplanar realization of the circuit because in this case the optimal impedance is about 120Ω and the impedance 50Ω even cannot be realized.

Fig. 23 presents the strip and slot widths of the 50Ω coplanar line on the *Alumina* substrate. The slot width versus the strip width is approximately a linear function. Larger coplanar line dimensions will be used near the input and output connectors.

4.2.3 Slot line

Fig. 20 shows a cross-section of a slot line.

Slot-line is not an attractive line for modelling using ideal transmission lines, used in the project. The line is highly dispersive and the characteristic impedance is not precisely defined. The power-voltage characteristic impedance definition and the dispersive model have been used in the configurations used in the circuit. Fig. 24 shows the slot-line impedance on *EPSILAM* and *Alumina* substrates for fixed slot width as a function of frequency. Slot lines are used only in the F0-10 low pass filter. Since the characteristics of this filter have to be considered only in the frequency range 0-15GHz, the characteristics of the impedance dispersion are interesting for this range only. The only slot line impedance used in the project is 50Ω. It is approximated by 50μm slot line on *ESPILAM* and 40μm slot line on *Alumina*. It has been tested by simulation that the characteristics of the filters

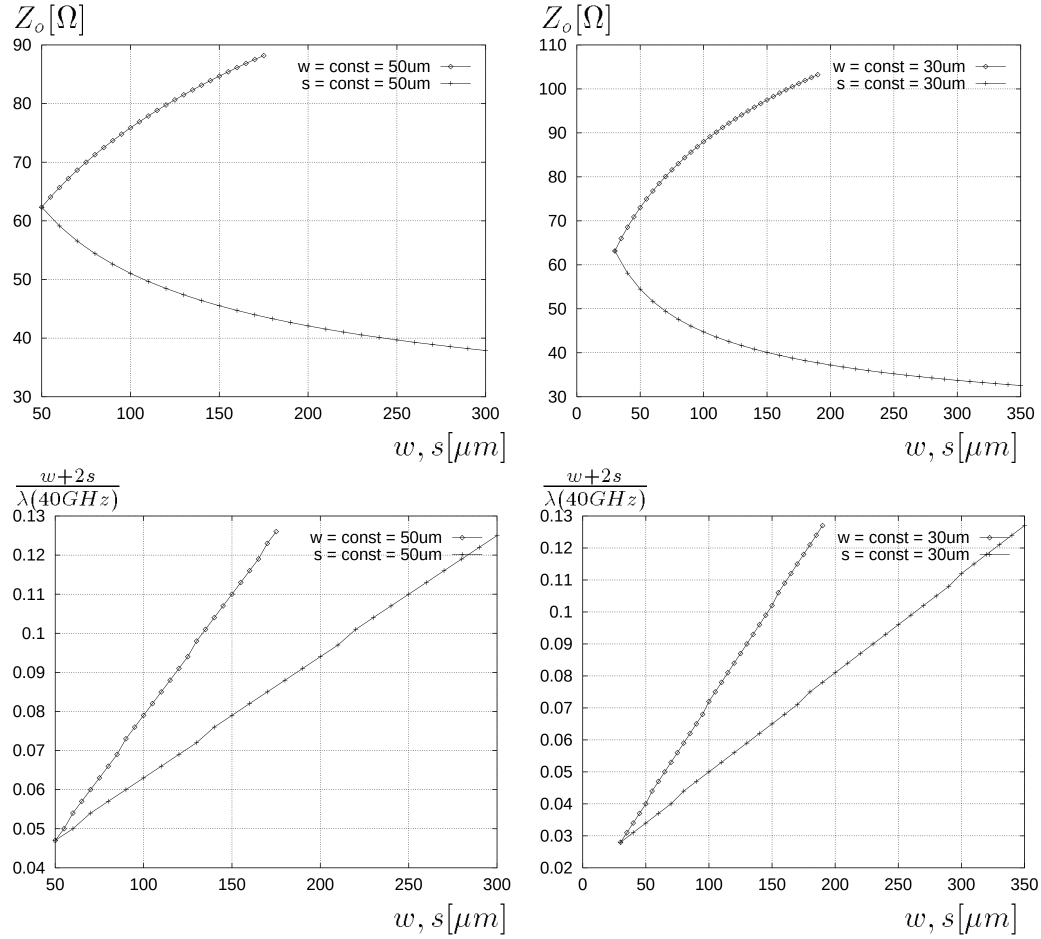

(a) (b)

Figure 21: *Coplanar line impedance and ratio of transverse line dimension to the wavelength at 40GHz versus strip and slot widths. Substrates: EPSILAM, $\epsilon_r = 10.2$, $h = 635\mu m$, $t = 20\mu m$ (a) and Alumina, $\epsilon_r = 9.9$, $h = 635\mu m$, $t = 10\mu m$ (b).*

are not sensitive to the impedance change in the range from the dispersive characteristics in Fig. 24.

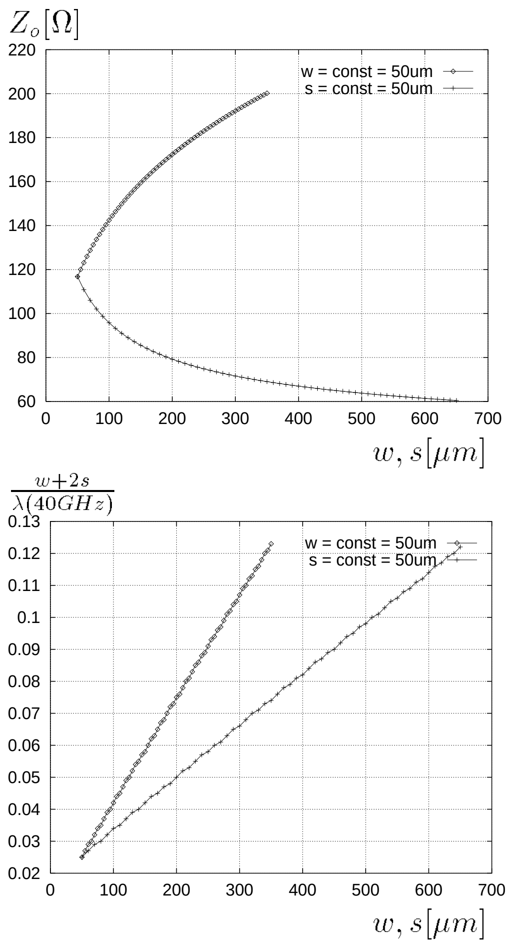

Figure 22: *Coplanar line impedance and ratio of transverse line dimension to the wavelength at 40GHz versus strip and slot widths. Substrate: DUROID,* $\epsilon_r = 2.2$, $h = 254\mu m$, $t = 20\mu m$

$w[\mu m]$	$s[\mu m]$	$Z_0[\Omega]$	$\frac{w+2s}{\lambda(40GHz)}$	$w[\mu m]$	$s[\mu m]$	$Z_0[\Omega]$	$\frac{w+2s}{\lambda(40GHz)}$
300	50	37.9	0.125	**50**	**50**	**62.3**	**0.047**
290	50	38.2	0.122	50	55	64.1	0.050
280	50	38.5	0.119	50	60	65.7	0.054
270	50	38.9	0.116	50	65	67.2	0.057
260	50	39.3	0.113	50	70	68.6	0.060
250	50	39.7	0.110	50	75	70.0	0.063
240	50	40.1	0.107	50	80	71.3	0.066
230	50	40.5	0.104	50	85	72.5	0.069
220	50	41.0	0.101	50	90	73.7	0.073
210	50	41.5	0.097	50	95	74.8	0.076
200	50	42.1	0.094	50	100	75.9	0.079
190	50	42.7	0.091	50	105	76.9	0.082
180	50	43.3	0.088	50	110	77.9	0.085
170	50	44.0	0.085	50	115	78.8	0.088
160	50	44.7	0.082	50	120	79.8	0.091
150	50	45.5	0.079	50	125	80.6	0.094
140	50	46.4	0.076	50	130	81.5	0.098
130	50	47.4	0.072	50	135	82.3	0.101
120	50	48.5	0.069	50	140	83.1	0.104
110	50	49.7	0.066	50	145	83.9	0.107
100	50	51.0	0.063	50	150	84.7	0.110
90	50	52.6	0.060	50	155	85.4	0.113
80	50	54.4	0.057	50	160	86.1	0.116
70	50	56.6	0.054	50	165	86.8	0.119
60	50	59.1	0.050	50	170	87.5	0.123
50	**50**	**62.3**	**0.047**	50	175	88.2	0.126

Table 14: *Coplanar line impedance and ratio of transverse line dimension to the wavelength at 40GHz versus strip and slot widths. Substrate: EPSILAM,* $\epsilon_r = 10.2$, $h = 635\mu m$, $t = 20\mu m$

$w[\mu m]$	$s[\mu m]$	$Z_0[\Omega]$	$\frac{w+2s}{\lambda(40GHz)}$	$w[\mu m]$	$s[\mu m]$	$Z_0[\Omega]$	$\frac{w+2s}{\lambda(40GHz)}$
350	30	32.6	0.127	**30**	**30**	**63.1**	**0.028**
340	30	32.8	0.124	30	35	66.0	0.031
330	30	33.0	0.121	30	40	68.6	0.034
320	30	33.2	0.118	30	45	70.9	0.037
310	30	33.5	0.115	30	50	73.0	0.040
300	30	33.7	0.112	30	55	75.0	0.044
290	30	34.0	0.108	30	60	76.8	0.047
280	30	34.3	0.105	30	65	78.5	0.050
270	30	34.6	0.102	30	70	80.1	0.053
260	30	34.9	0.099	30	75	81.6	0.056
250	30	35.2	0.096	30	80	83.0	0.059
240	30	35.6	0.093	30	85	84.3	0.062
230	30	35.9	0.090	30	90	85.6	0.065
220	30	36.3	0.087	30	95	86.8	0.068
210	30	36.8	0.084	30	100	88.0	0.072
200	30	37.2	0.081	30	105	89.1	0.075
190	30	37.7	0.078	30	110	90.2	0.078
180	30	38.2	0.075	30	115	91.2	0.081
170	30	38.8	0.071	30	120	92.2	0.084
160	30	39.4	0.068	30	125	93.2	0.087
150	30	40.1	0.065	30	130	94.1	0.090
140	30	40.8	0.062	30	135	95.0	0.093
130	30	41.6	0.059	30	140	95.8	0.096
120	30	42.5	0.056	30	145	96.7	0.099
110	30	43.6	0.053	30	150	97.5	0.102
100	30	44.7	0.050	30	155	98.3	0.106
90	30	46.1	0.047	30	160	99.0	0.109
80	30	47.6	0.044	30	165	99.8	0.112
70	30	49.4	0.040	30	170	100.5	0.115
60	30	51.7	0.037	30	175	101.2	0.118
50	30	54.5	0.034	30	180	101.9	0.121
40	30	58.1	0.031	30	185	102.6	0.124
30	**30**	**63.1**	**0.028**	30	190	103.2	0.127

Table 15: *Coplanar line impedance and ratio of transverse line dimension to the wavelength at 40GHz versus strip and slot widths. Substrate: Alumina,* $\epsilon_r = 9.9$, $h = 635\mu m$, $t = 10\mu m$ *(b).*

$Z_0 = 50\Omega$	
$w[\mu m]$	$s[\mu m]$
70	30
80	40
180	80
280	120
400	170
500	200

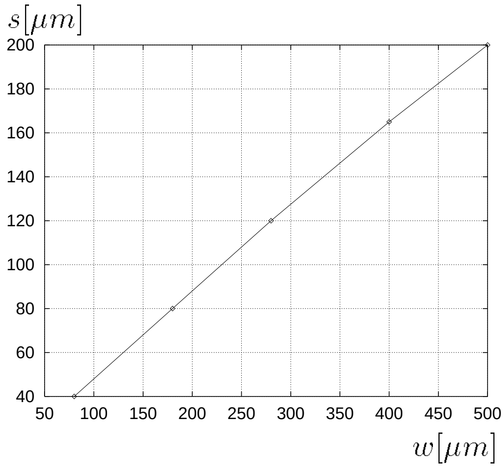

Figure 23: *Strip (w) and slot (s) widths of the* 50Ω *coplanar line. Substrate: Alumina,* $\epsilon_r = 9.9$*,* $h = 635\mu m$*,* $t = 10\mu m$*.*

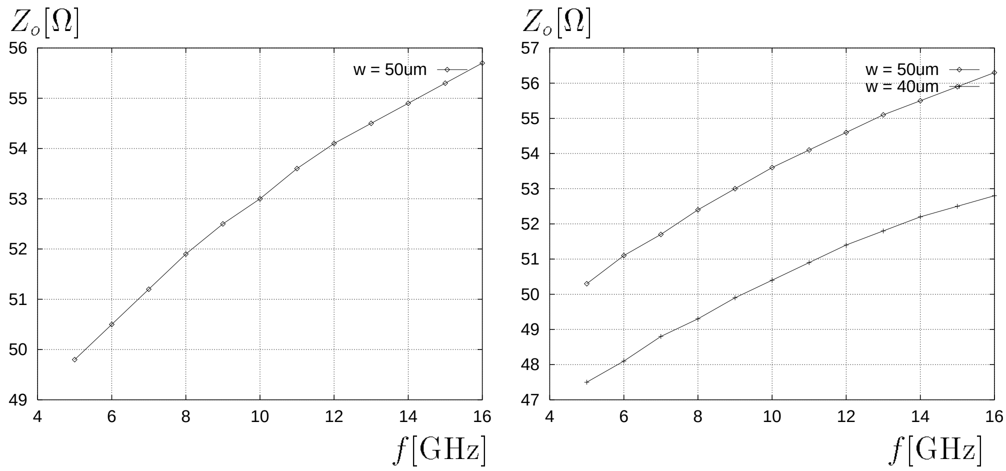

(a) (b)

Figure 24: *Slot line impedance as a function of frequency. Substrates: EPSILAM,* $\epsilon_r = 10.2$*,* $h = 635\mu m$*,* $t = 20\mu m$ *(a) and Alumina,* $\epsilon_r = 9.9$*,* $h = 635\mu m$*,* $t = 10\mu m$ *(b).*

4.3 Distributed elements

The following distributed elements have been considered in the design of the filters:

- Transmission lines in cascade
- Parallel open stub
- Parallel shunted stub
- Serial open stub
- Serial shunted stub

4.3.1 Transmission lines in cascade

The coplanar realization of a transmission line, and its idealized model are shown in Fig. 25.

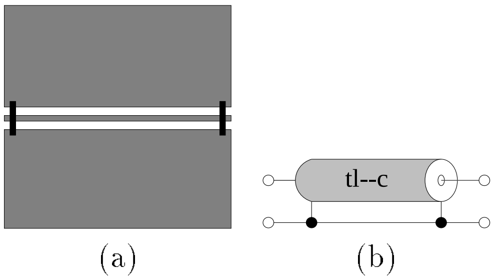

Figure 25: *Coplanar line in cascade (a) and its idealized model (b)*

The input impedance of the inserted transmission line is given by:

$$Z_{in} = Z_0 \frac{Z_L + jZ_0 \tan\Theta}{Z_0 + jZ_L \tan\Theta} \tag{67}$$

where

Z_0	-	characteristic transmission line impedance,
Θ	-	transmission line electrical length,
Z_L	-	load impedance.

Cascade transmission lines are used in every type of filters as impedance transformers.

4.3.2 Parallel open stub

The coplanar realization of a parallel open stub, and its idealized model are shown in Fig. 26.

The input impedance of an open stub is given by:

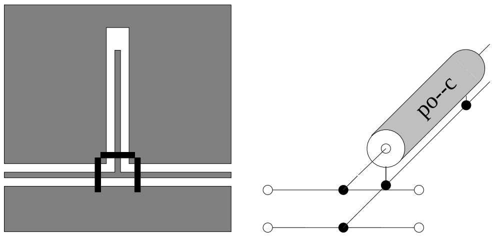

Figure 26: *Open parallel coplanar stub (a) and its idealized model (b)*

$$Z_o = -jZ_0 \cot \Theta \tag{68}$$

where Z_0 is the characteristic impedance, and Θ is the electrical length of the stub. Fig. 27 shows two parallel open stubs with the same characteristic impedances.

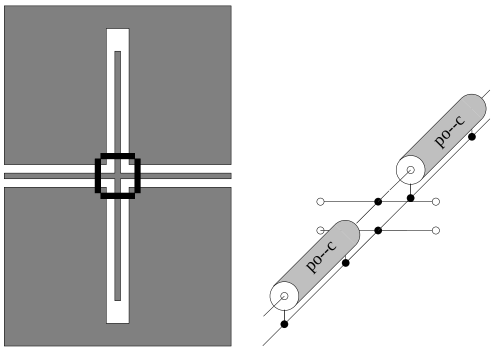

Figure 27: *Open parallel coplanar stubs (a) and their idealized model*

Stubs connected in parallel are electrically equivalent to one stub with the characteristic admittance being the sum of characteristic admitances of the stubs. Therefore, the input impedance of such a structure is given by:

$$Z_{2o} = -j\frac{1}{2}Z_0 \cot \Theta = \frac{1}{2}Z_o \tag{69}$$

Since the characteristic impedance range 50–75Ω has been chosen for coplanar transmission lines (see Sect. 4.2.1), there are two ranges of the coplanar stubs characteristic impedances: 50–75Ω (one stub) and 25–37Ω (two stubs).

From (68) and the properties of the *cotangent* function:

- $Z_{os} = 0$ for $\Theta = (2n+1) \cdot 90^o$, with n being an integer.

  An open circuit is transformed to a shunt. In the case of the parallel stub it implies the total reflection of the signal.

- $Z_{os} = \infty$ for $\Theta = n \cdot 180^o$, with n being an integer.

  The stub has properties of an open circuit. In the case of the parallel stub it implies passing of the total signal.

Parallel open stubs may be used as low-pass elements, as well as band-pass elements, in the bands where the stub has the electrical length being a multiple of 180^o at the middle frequencies. In the later case, however, there is a parasitic band or bands below the band of interest where the stub is also a pass element. Additional stubs of different kind should be used to eliminate these bands.

4.3.3 Parallel shunted stub

The coplanar realization of a parallel shunted stub, and its idealized model are shown in Fig. 28.

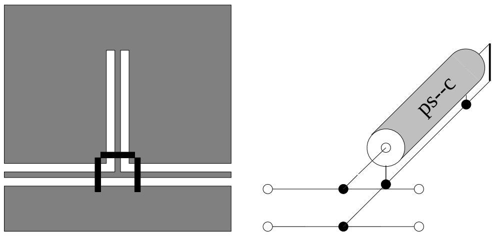

(a) (b)

Figure 28: *Shunted parallel coplanar stub (a) and its idealized model (b)*

The input impedance of a shunted stub is given by:

$$Z_s = jZ_0 \tan \Theta \tag{70}$$

where Z_0 is the characteristic impedance, and Θ is the electrical length of the stub. Fig. 29 shows two parallel shunted stubs with identical characteristic impedances. Analogically to (69) the input impedance of such a structure is given by:

$$Z_{2s} = j\frac{1}{2}Z_0 \tan \Theta = \frac{1}{2}Z_s \tag{71}$$

There are two ranges of the coplanar stubs characteristic impedances: 50–75Ω (one stub) and 25–37Ω (two stubs).

From (70) and the properties of the *tangent* function:

- $Z_{os} = \infty$ for $\Theta = (2n+1) \cdot 90^o$, with n being an integer.

  A shunt is transformed to an open circuit. In the case of the parallel stub it implies passing of the total signal.

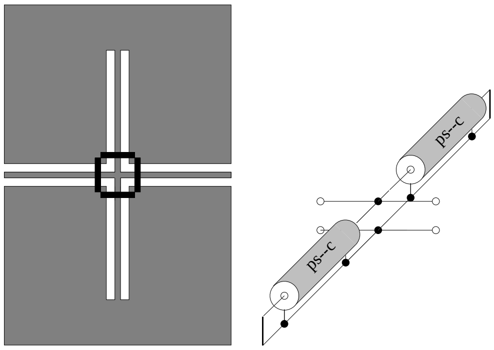

(a) (b)

Figure 29: *Shunted parallel coplanar stubs (a) and their idealized model (b)*

- $Z_{os} = 0$ for $\Theta = n \cdot 180^o$, with n beeing an integer.

  The stub has properties of a shunt. In the case of the parallel stub it implies the total reflection of the signal.

Parallel shunted stubs may be used as band-pass elements, in the bands where at the center frequencies the stub has the electrical length $(2n+1) \cdot 90^o$, with n being an integer. If $n > 1$ there is a parasitic band or bands below the band of interest where the stub is also a pass element. Additional stubs should be used to eliminate these bands.

4.3.4 Serial shunted stub

The serial stubs are realized in the uniplanar technology as slot-lines (Sect. 4.2.3). A symmetric configuration of two slots is used as shown in Fig. 30.

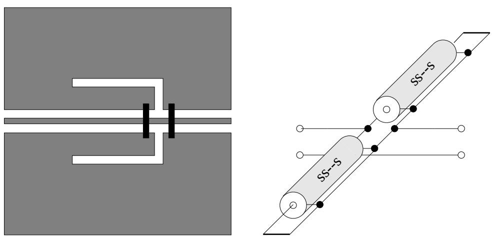

(a) (b)

Figure 30: *Shunted serial slot stubs (a) and their idealized model (b)*

The electrical response of a straight double slot line resonator may be inferior in comparison to the bent geometry since the two slots, with electrical fields oriented in phase, work as a slot antenna (see [5]). In the bent geometry the electrical fields are out-of-phase, which reduces radiation loss.

The input impedance of two slots is given by (71). Like parallel open stubs, serial shunted stubs may be used as low-pass elements, as well as band-pass elements, in the bands where at the middle frequencies the stub has the electrical length being a multiple of 180^o. In the later case, however, there is a parasitic band or bands below the band of interest, where the stub is also a pass element. Additional stubs of different kind should be used to eliminate these bands

4.3.5 Serial open stub

A serial open stub has not been used in the circuit because of the problems with realization of a wide-band open circuit in a slot line.

4.3.6 Conditions for modelling

Using the elements presented in Sect. 4.3, there is a lot of possible topologies of the filters satisfying the conditions for modelling. After choosing one of them, the impedances of the transmission lines (the cascade lines and the stubs) become the subject of optimization. Choosing different topologies we can achieve different sets of impedances.

In the simulations, very simple models have been used, based on ideal transmission lines without considering the influence of discontinuities and dispersion. For this reason it was very important to minimize the discontinuities in the circuit. Therefore, the values of the impedances are not only limited by the capability of the technology. The stronger condition is minimization of discontinuities. To satisfy this condition all the impedances used should be close to the values optimal for a given substrate. Some examples of discontinuities which appear in the project are shown in Fig. 31.

The minimization of the influence of these discontinuities on the circuit characteristics is achieved by minimization of their dimensions, i.e. the minimization of the transmission lines slot and strip widths. In other words, an optimal impedance range has been chosen for every substrate in the planar realization of the circuit, where the transverse dimensions of the lines are minimal (see Sect. 4.2.1).

As the results of the measurements show, this simple modelling provides good results within desired frequency range, provided that the discontinuity minimization condition is satisfied.

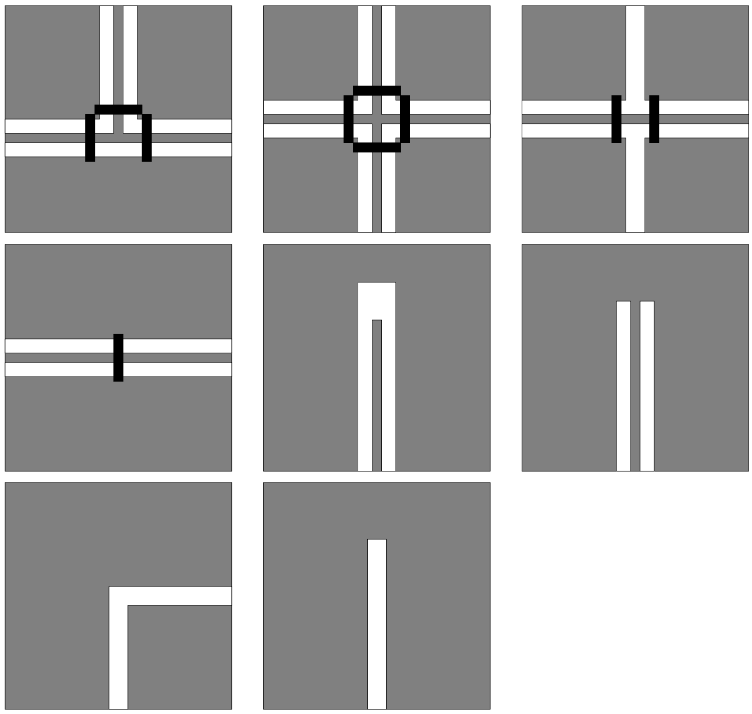

Figure 31: *Examples of discontinuities in the uni-planar technology*

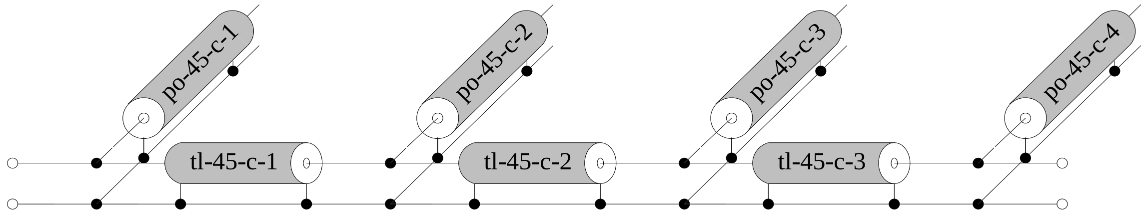

Figure 32: *Idealized model of F0-15 low pass filter*

4.4 F0-15 low pass filter

4.4.1 Modelling

The conditions which the low pass F0-15 filter should satisfy are:

- Pass band: 0-15GHz
- Maximal attenuation in the pass band: 0.25dB
- Stop band: 20-40GHz
- Minimal attenuation in the stop band: 20dB
- The reflection coefficient in the stop band should approximate a shunt

All of these points are the conditions for the optimization of the filter. An idealized model of the filter given in Fig. 32 shows the filter topology which has been chosen. The electrical length of all the stubs and cascade lines used is 90^o at 30GHz. Therefore the biggest attenuation of the filter is near 30GHz and the characteristic is symmetric around this frequency.

The circuit has been optimized for various number of stubs, giving different optimal characteristics. The smallest number of stubs that gives satisfying characteristics of the filter is 4.

The optimal transmission and reflection characteristics are shown in Fig. 33. The minimal attenuation in the stop-band of the filter is 25dB at 20GHz and 40GHz. The maximal attenuation in the pass-band of the filter is 0.25dB.

Tab. 16 shows the optimal impedances of the elements of the filter. The impedance of the **po-45-c-2** and **po-45-c-2** stubs is 27Ω and since the range of the available impedances is 50Ω–75Ω they are split into two stubs with the impedance two times larger (see Sect. 4.3.2), which is 54Ω.

4.4.2 Realization and measurements

A test circuit of the F0-15 low pass filter has been realized on *Alumina* substrate, $\epsilon_r = 9.9$, $h = 635\mu m$, $t = 10\mu m$ (see Fig. 35). Fig. 34 shows the results of the measurements of this circuit. Very good agreement with the simulation results may be observed. The highest attenuation in the pass-band is about 2dB at 15GHz.

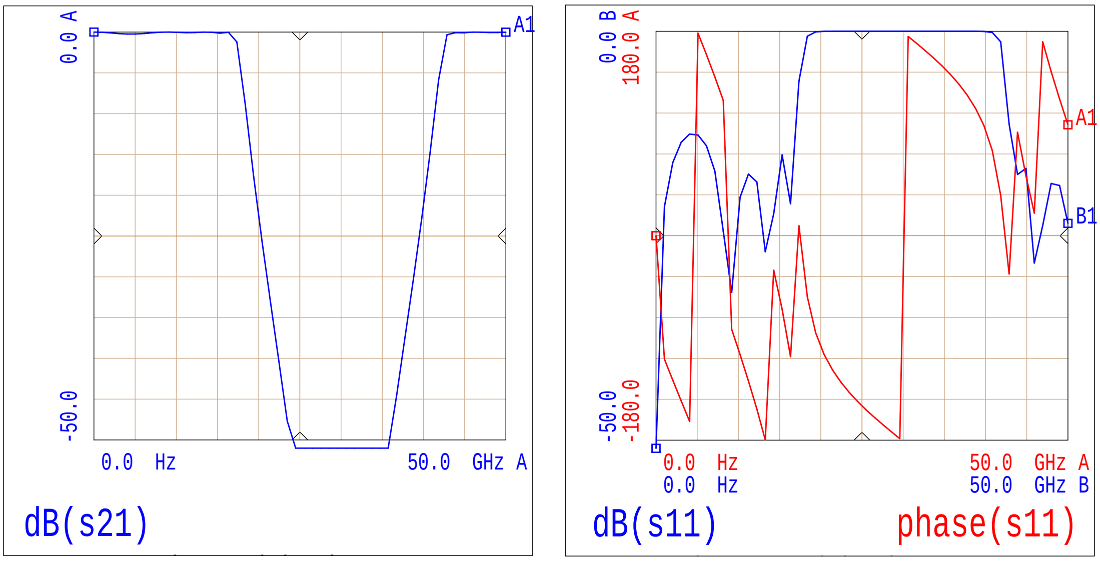

(a) (b)

Figure 33: *Transmission (a) and reflection (b) of F0-15 low pass filter – results of the optimization*

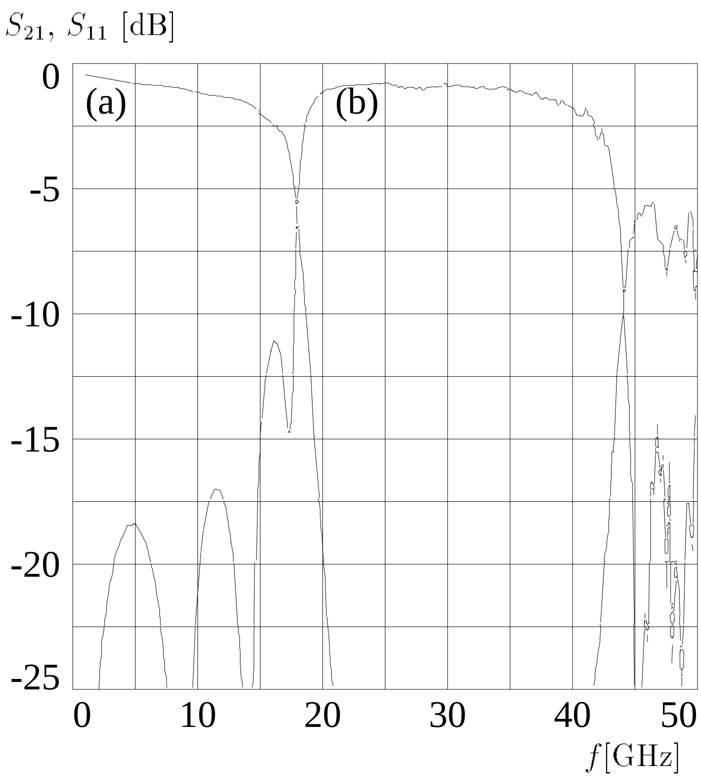

Figure 34: *Measured transmission (a) and reflection (b) of F0-15 low pass filter*

Element	Z_0 [Ω]	*EPSILAM* s [μm]	*EPSILAM* w [μm]	*Alumina* s [μm]	*Alumina* w [μm]
po-45-c-1 po-45-c-4	50	50	110	30	70
tl-45-c-1 tl-45-c-3	75	95	50	55	30
po-45-c-2 po-45-c-3	27	–	–	–	–
po-45-c-2a po-45-c-2b po-45-c-3a po-45-c-3b	54	50	80	30	50
tl-45-c-2	75	95	50	55	30
50Ω line	50	50	110	30	70
(probe)		–	–	40	80

Electrical length at 15GHz [^{o}]	Physical length [μm] *EPSILAM*	Physical length [μm] *Alumina*
45	1050	1070

Table 16: *Impedances of the elements of F0-15 low pass filter – results of the optimization*

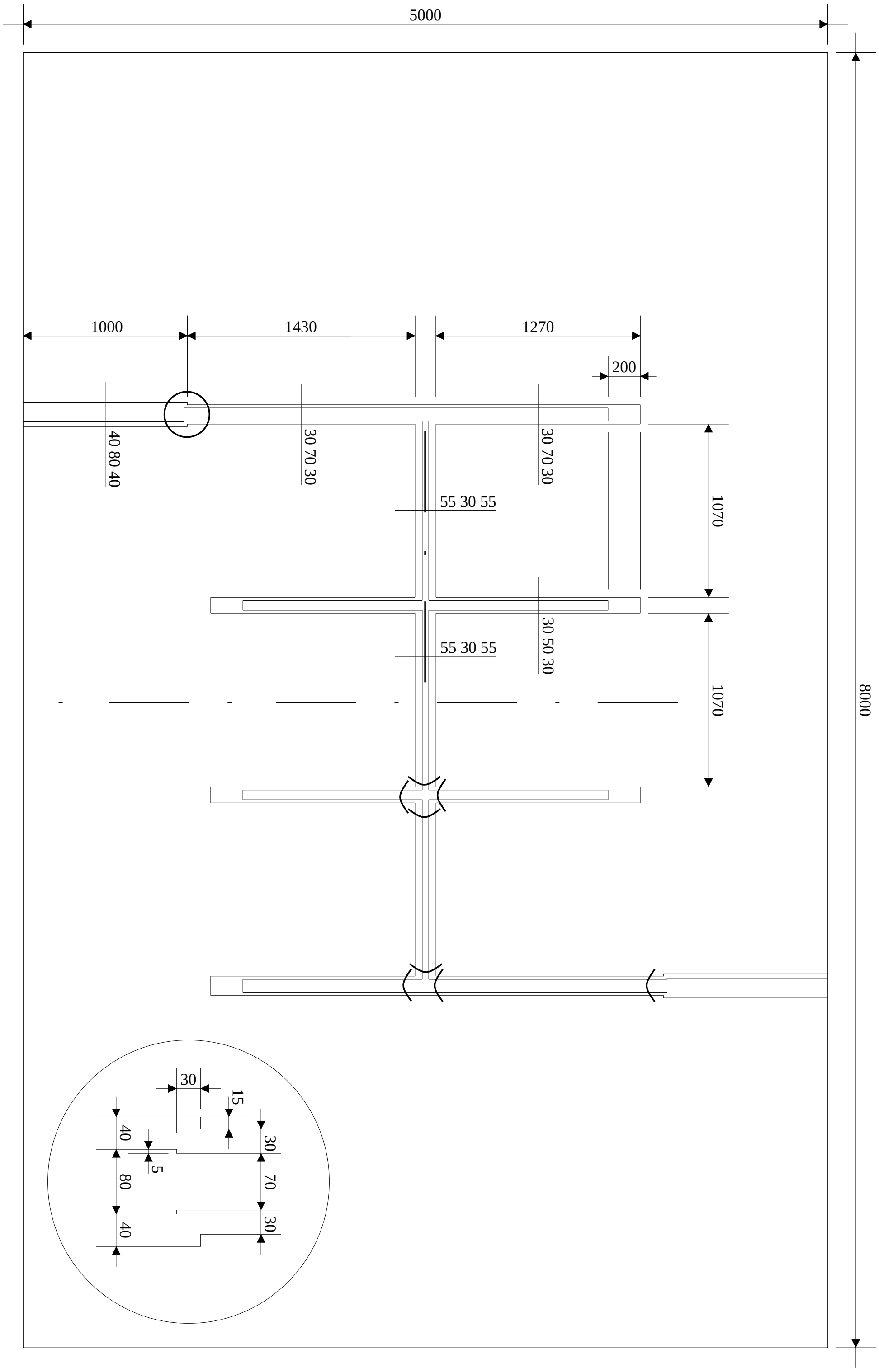

Figure 35: *The F0-15 low pass filter – test circuit realized in the coplanar technology. Substrate: Alumina, $\epsilon_r = 9.9$, $h = 635\mu m$, $t = 10\mu m$. All dimensions in μm.*

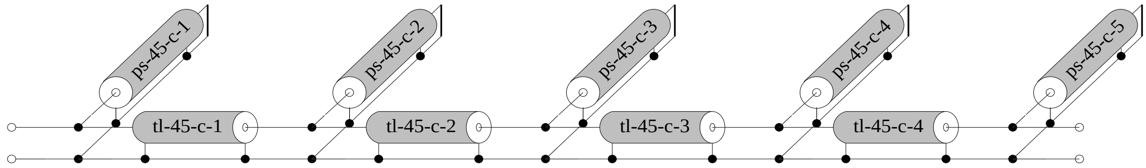

Figure 36: *Idealized model of F20-40 band pass filter*

4.5 F20-40 band pass filter

4.5.1 Modelling

The conditions that the band pass F20-40 filter should satisfy are:

- Pass band: 20-40GHz
- Maximal attenuation in the pass band: 0.25dB
- Stop band: 0-15GHz
- Minimal attenuation in the stop band: 20dB
- The reflection coefficient in the stop band should approximate a shunt

All of these points are the conditions for the optimization of the filter. An idealized model of the filter given in Fig. 36 shows the topology of the filter which has been chosen. The electrical length of all the stubs and cascade lines used is 90^o at 30GHz. Therefore the attenuation at 30GHz is zero and the characteristics is symmetric around this frequency.

The circuit has been optimized for various number of stubs, giving different optimal characteristics. The smallest number of stubs that gives satisfying characteristics of the filter is 5.

The optimal transmission and reflection characteristics are shown in Fig. 37. The minimal attenuation in the stop-band of the filter is 20dB at 15GHz and 45GHz. The maximal attenuation in the pass-band of the filter is 0.2dB.

Tab. 17 shows optimal impedances of the elements of the filter. The impedance of the **ps-45-c-1** and **ps-45-c-5** stubs is 33Ω and since the range of the available impedances is 50Ω–75Ω they are split into two stubs with the impedance two times larger (see Sect. 4.3.3), which is 66Ω.

4.5.2 Realization and measurements

A test circuit of F20-40 band pass filter has been realized on *Alumina* substrate (see Fig. 39). Fig. 38 shows the results of the measurements of this circuit. Very good agreement with the simulation results may be observed. The attenuation in the pass-band is about 2–4dB.

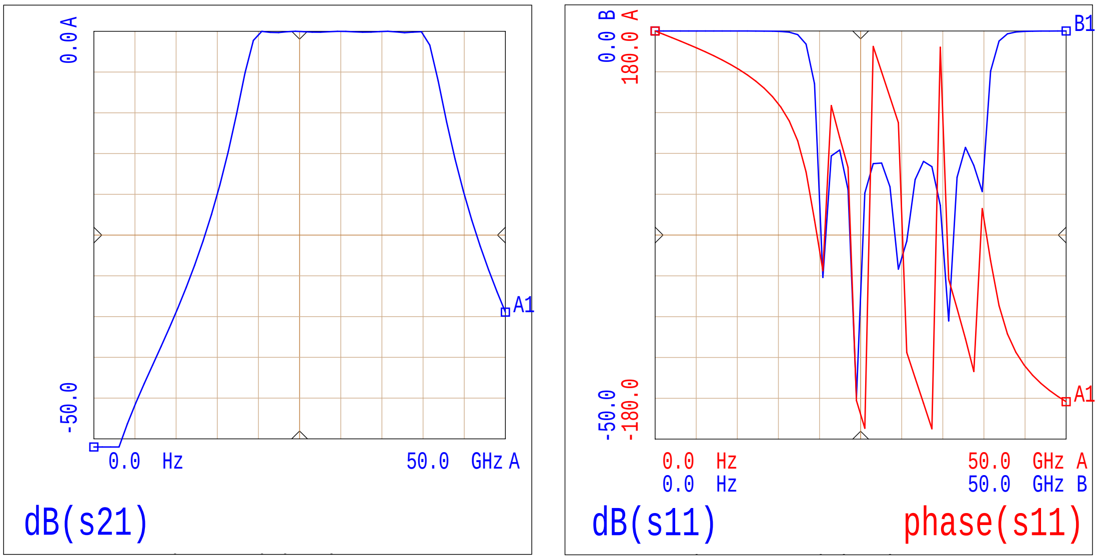

(a) (b)

Figure 37: *Transmission (a) and reflection (b) of F20-40 band pass filter, results of the optimization*

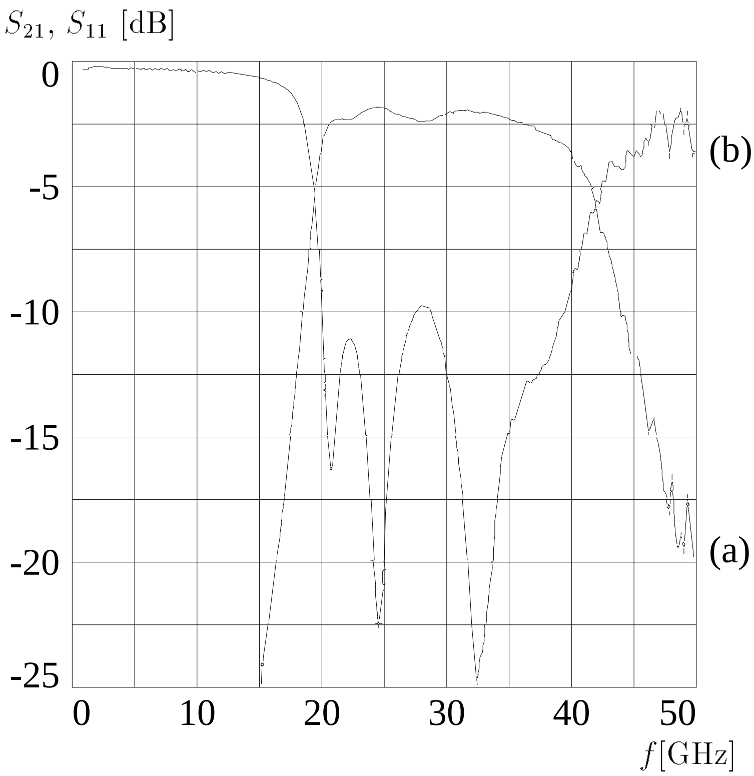

Figure 38: *Measured transmission (a) and reflection (b) of F20-40 band pass filter*

Element	Z_0 [Ω]	*EPSILAM* s [μm]	*EPSILAM* w [μm]	*Alumina* s [μm]	*Alumina* w [μm]
ps-45-c-1 ps-45-c-5	33	–	–	–	–
ps-45-c-1a ps-45-c-1b ps-45-c-5a ps-45-c-5b	66	60	50	35	30
tl-45-c-1 tl-45-c-4	52	50	90	30	60
ps-45-c-2 ps-45-c-4	52	50	95	30	60
tl-45-c-2 tl-45-c-3	70	75	50	45	30
ps-45-c-3	58	50	60	30	40
50Ω line	50	50	110	30	70
(probe)		–	–	40	80

Electrical length at 15GHz [^{o}]	Physical length [μm] *EPSILAM*	Physical length [μm] *Alumina*
45	1050	1070

Table 17: *Impedances of the elements of F20-15 band pass filter – results of the optimization*

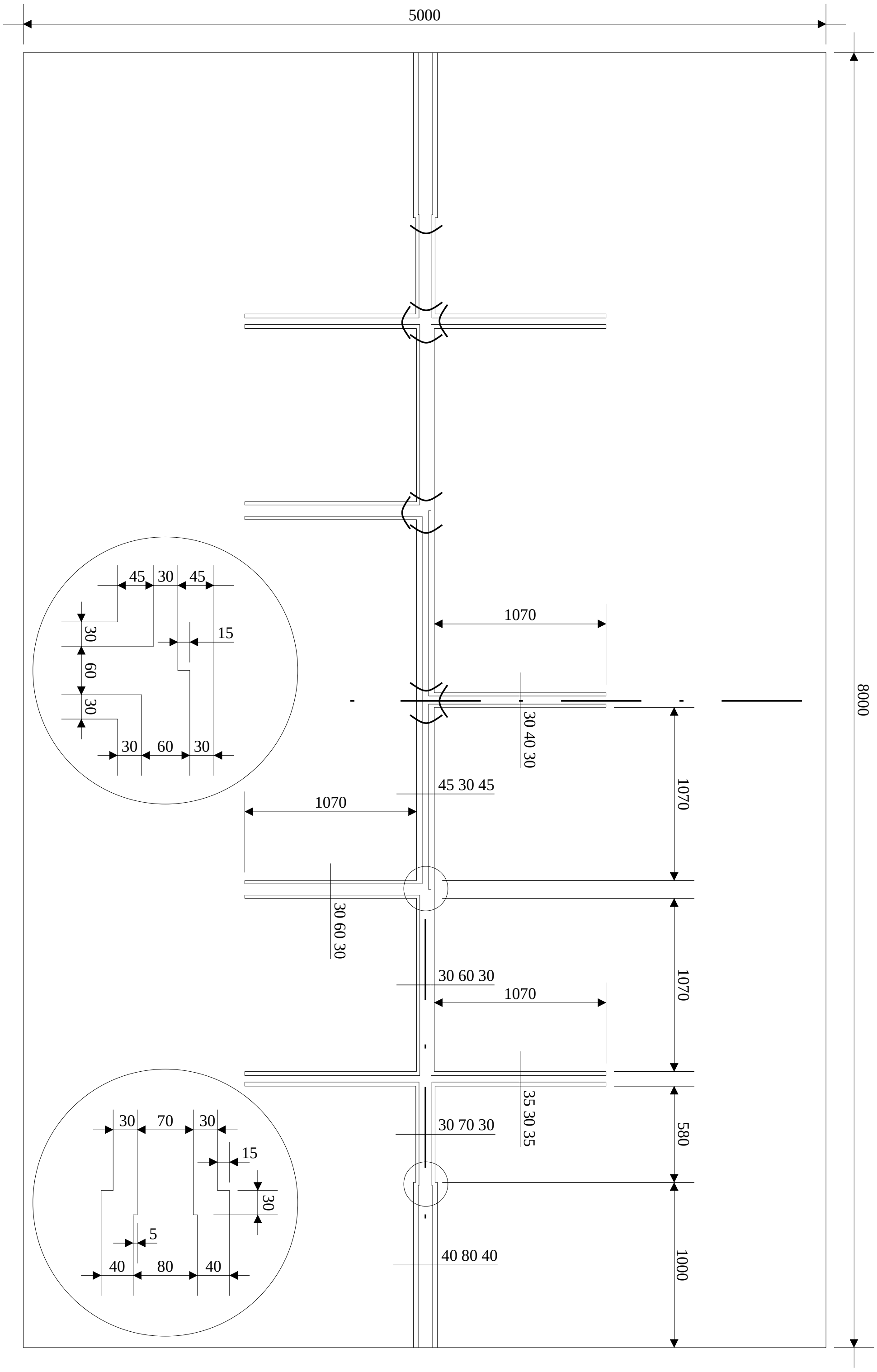

Figure 39: *F20-40 band pass filter – test circuit realized in the coplanar technology. Substrate: Alumina,* $\epsilon_r = 9.9$, $h = 635\mu m$, $t = 10\mu m$. *All dimensions in* μm.

4.6 F0-10 low pass filter and F15 band pass filter

As we saw in the last chapters, we may choose the impedances of all the transmission lines from the range optimal for a given substrate, minimizing the discontinuities, so their influence on the characteristics of the filters is not important in the interesting band 0–40GHz. Since the work-band of the filters F0-10 and F0-15 is just 0–15GHz and we are going to use the same range of impedances of the transmission lines as in the case of the filters F0-15 and F20-40, we should achieve good results by using the same simple method of the circuit design.

4.6.1 Interconnection between F0-10 and F15 filters

The biggest problem with the filters F0-10 and F15 is the interconnection between them. Therefore they should be analized together. Besides the conditions of how the transmission characteristics of the filters should look like, additional conditions appear for the configuration and the reflection coefficients in the stop-bands of the filters in the plane of interconnection. If we are able to satisfy such conditions, the optimizations of the impedances of the transmission lines may be done independently for two filters.

The topology of F0-10 low pass filter is shown in Fig. 40. The port *3* of the filter is connected to the F15 band pass filter. The element **tl-90-s** should work as a serial shunted stub in the pass band of the F0-10 filter (0-10GHz). Therefore F15 filter should approximate a shunt in this band. This is a condition for optimization of this filter.

The transition of the signal from the port *3* to *2* of the F0-10 filter should be assured in the pass-band of F15 band pass filter. Since this band is very narrow, near 15GHz, it is easy to satisfy this condition by choosing an appropriate topology of F0-10 filter. The following conditions should be satisfied:

- **tl-90-s**'s impedance should be 50Ω
- **ss-90-s-3** serial shunted stub should be an open circuit near 15GHz. Therefore its electrical length is set to 90^o at this frequency (see Sect. 4.3.4).
- **po-90-c** parallel open stub should be a shunt near 15GHz. Therefore its electrical length is set to 90^o at this frequency (see Sect. 4.3.2).

The model of F0-10 and F15 filters connected together is shown in Fig. 42 The element **tl-90-s** is a slot line in the planar realization of the circuit. Since the ports of the F15 filter are coplanar a transition from the slot to coplanar standard is needed. Fig. 43 shows such transition and its idealized model. The modified circuit of the F0-10 and F15 filters is shown in Fig. 44. The additional element **ps-90-s** represents the slot-to-coplanar transition. It was tested that this change of the topology has no significant influence on the characteristics of the circuit in the desired band. The transmission characteristics of a modified idealized model of F15 and F0-10 filters, connected together, are shown in Fig. 47.

4.6.2 F0-10 low pass filter

The conditions that the low pass F0-10 filter should satisfy are:

- Pass band: 0-10GHz
- Maximal attenuation in the pass band: 0.25dB
- Stop band: 15GHz

  Since the stop band is just a single frequency it is easy to satisfy this condition by choosing appropriate topology of the filter. A parallel open stub and serial shunted stubs, all of the length 90^0 at the frequency 15GHz have been used, so they satisfy this condition and it does not have to be considered during the optimization.
- Conditions on the topology of the filter which were presented in the Sect. 4.6.1

The topology of the filter is shown in Fig. 40. The serial shunted stubs are realized as slot lines. The 50Ω impedance has been fixed for all of these lines and it is not a subject of the optimization. The only optimized impedance is that of the parallel open stub. The results of the optimization show that to satisfy the first condition this impedance should be the highest possible. Since we have chosen an optimal impedance range for our substrates: 50Ω–75Ω, the realized impedance of the stub is 75Ω.

Fig. 45 shows the characteristics of the filter after optimization. Tab. 18 shows the optimal impedances of the elements of F0-10 and F15 filters.

4.6.3 F15 band pass filter

The conditions that the band pass F15 filter should satisfy are:

- Pass band: around 15GHz. The width of the band is not important, since this filter should pass only the local oscillator signal, which has a constant frequency 15GHz.
- Stop band: 0-10GHz
- Minimal attenuation in the stop band: 20dB
- The reflection coefficient in the stop band should approximate a shunt

All of these points are the conditions for the optimization of the filter. Various topologies have been considered during the optimization, giving different sets of optimal impedances of the lines and different degree of approximation. One of the best topologies found is shown in Fig. 41. Fig. 46 shows the characteristics of the filter after optimization. Tab. 18 shows the optimal impedances of the elements of F0-10 and F15 filters.

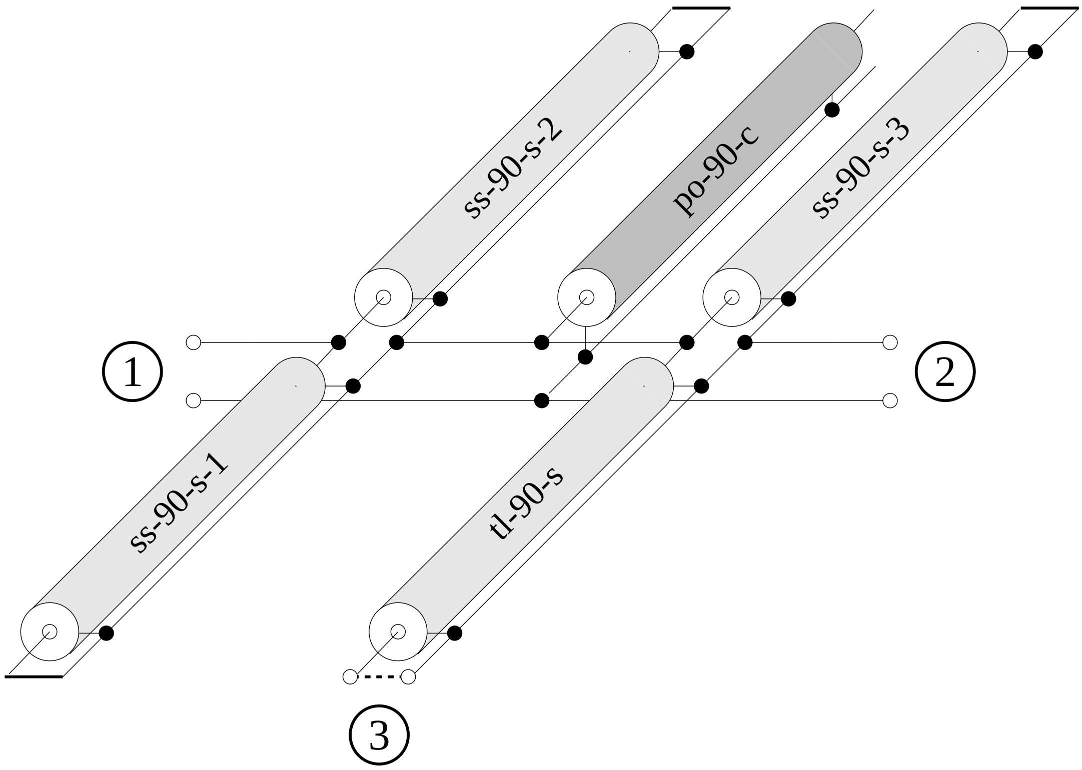

Figure 40: *Idealized model of the F0-10 low pass filter*

4.6.4 Realization and measurements

The test circuit of both filters F0-10 and F15 connected together has been realized on the *EPSILAM* substrate, $\epsilon_r = 10.2$, $h = 635\mu m$, $t = 20\mu m$ (see Fig. 48). Fig. 49 shows the results of the measurements of this circuit. Good agreement with the simulation results may be observed. Maximal attenuation in the F0-10 filter pass-band is about 2.5dB at 10GHz. The measured F15 filter characteristic has a resonance at about 15GHz, as predicted in the simulations. The minimal attenuation is about 5dB. The insertion losses should be much lower on *Alumina* substrate, since the material losses are much smaller in *Alumina* than in *EPSILAM*. Therefore *Alumina* was chosen for the realization of the final circuit.

	Element	Line	ϕ_{15} [^{o}]	Z_0 [Ω]	*EPSILAM* s [μm]	*EPSILAM* w [μm]	*Alumina* s [μm]	*Alumina* w [μm]
F0-10	po-90-c	copl.	90	75	95	50	45	30
	ss-90-s-1 ss-90-s-2 ss-90-s-3	slot	90	50	50	–	40	–
	tl-45-s	slot	45	50	50	–	40	–
	ps-90-s	slot	90	50	50	–	40	–
	tl-45-c-0	copl.	45	50	50	110	30	70
F15	ps-45-c-1 ps-45-c-2	copl.	45	25	–	–	–	–
	ps-45-c-1a ps-45-c-1b ps-45-c-2a ps-45-c-2b			50	50	110	30	70
	tl-45-c-1 tl-45-c-2	copl.	45	50	50	110	30	70
	po-45-c	copl.	45	60	50	60	30	40
	50Ω line	copl.		50	50	110	30	70

Line	Electrical length at 15GHz [^{o}]	Physical length [μm] *EPSILAM*	Physical length [μm] *Alumina*
copl.	45	1050	1070
	90	2100	2140
slot	45	1125	1135
	90	2250	2275

Table 18: *Impedances of the elements of the F0-10 low pass filter and the F15 band pass filter connected together – results of the optimization*

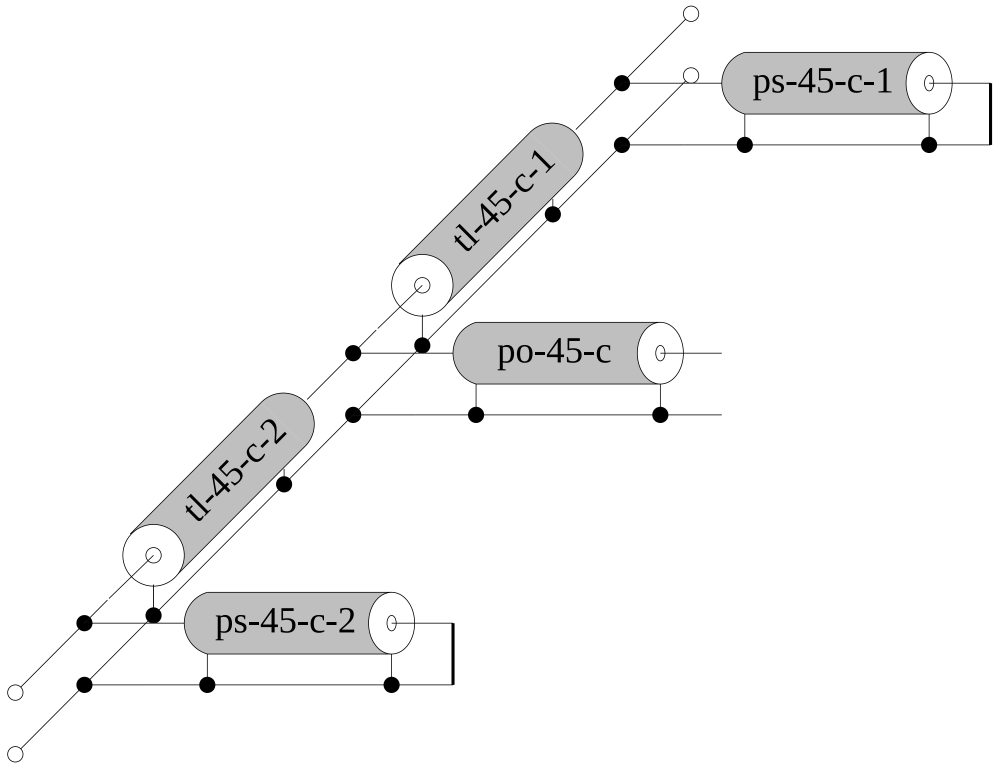

Figure 41: *Idealized model of the F15 band pass filter*

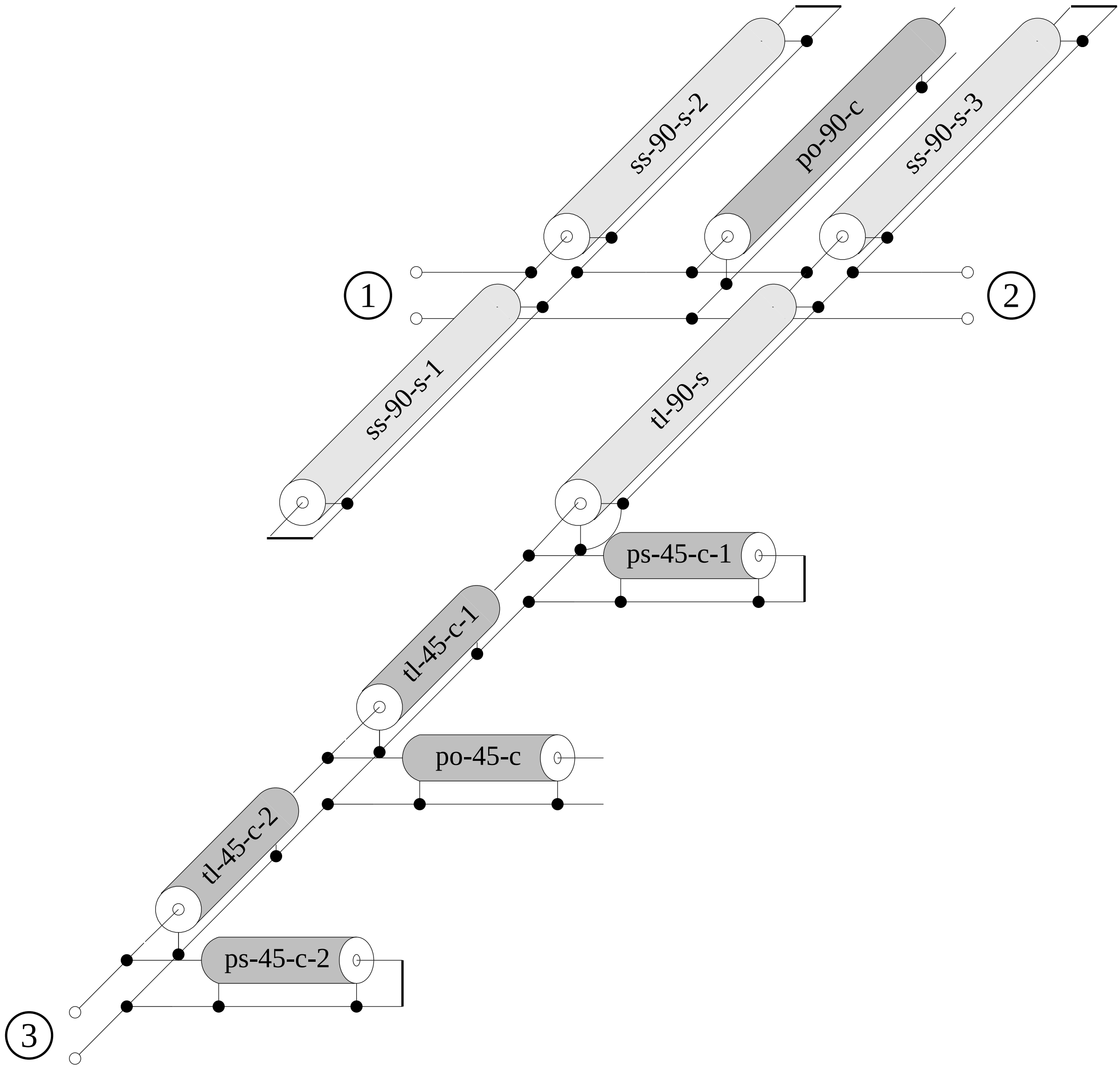

Figure 42: *Idealized model of the F0-10 low pass filter and the F15 band pass filter connected together*

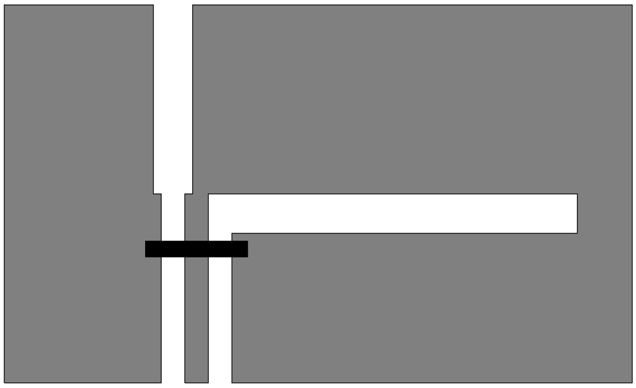

(a)

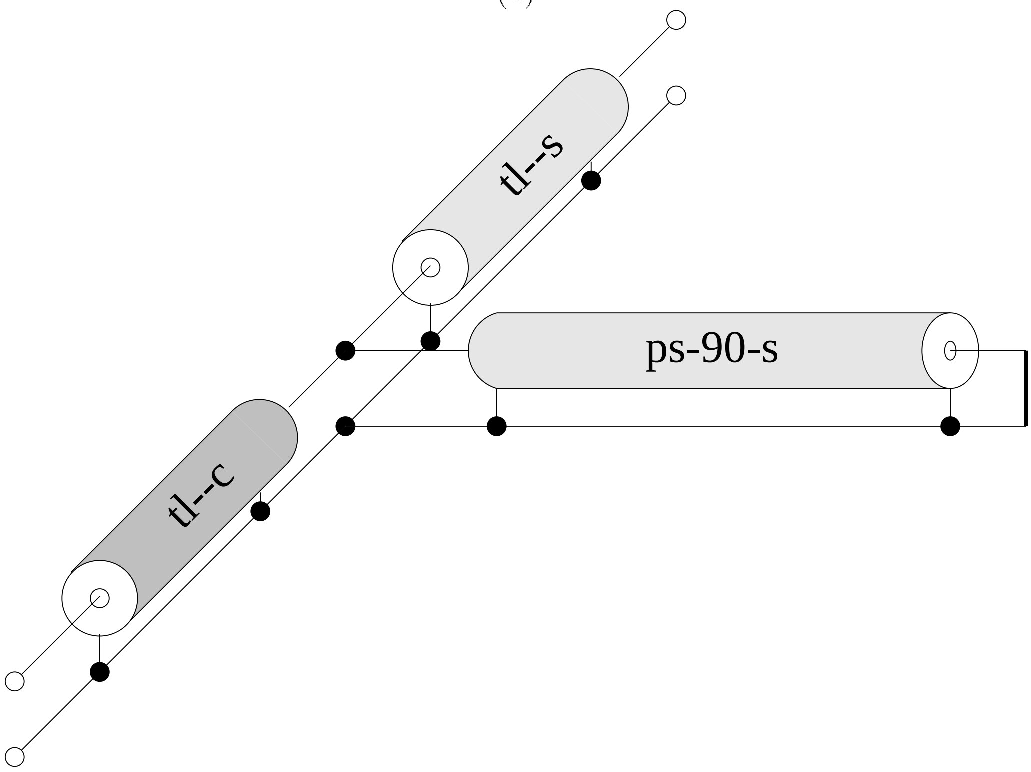

(b)

Figure 43: *Coplanar to slot line transition (a) and its idealized model (b)*

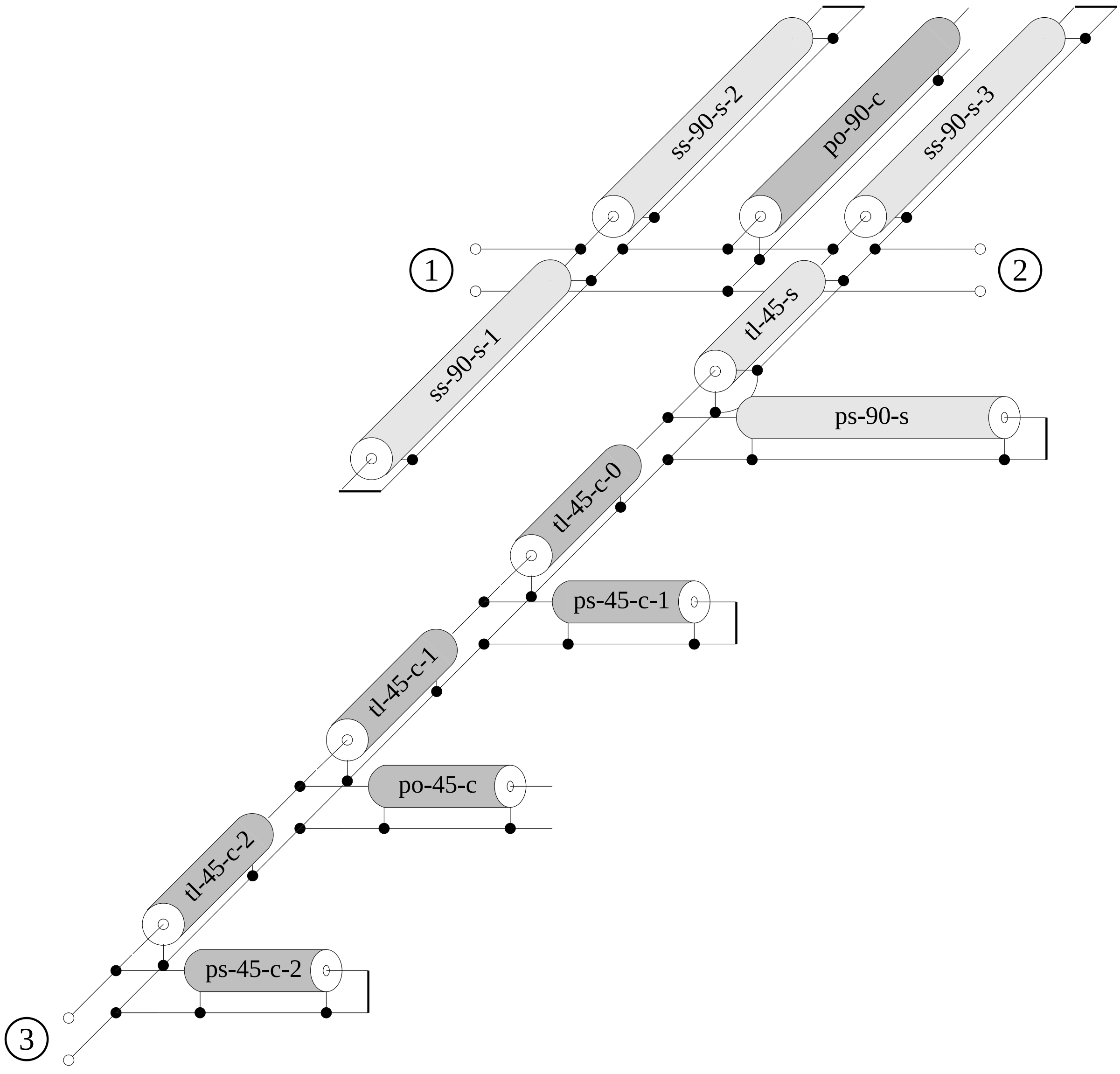

Figure 44: *Modified idealized model of the F0-10 low pass filter and the F15 band pass filter connected together. The additional parallel shunted slot stub* **ps-90-s** *represents the slot-to-coplanar line transition*

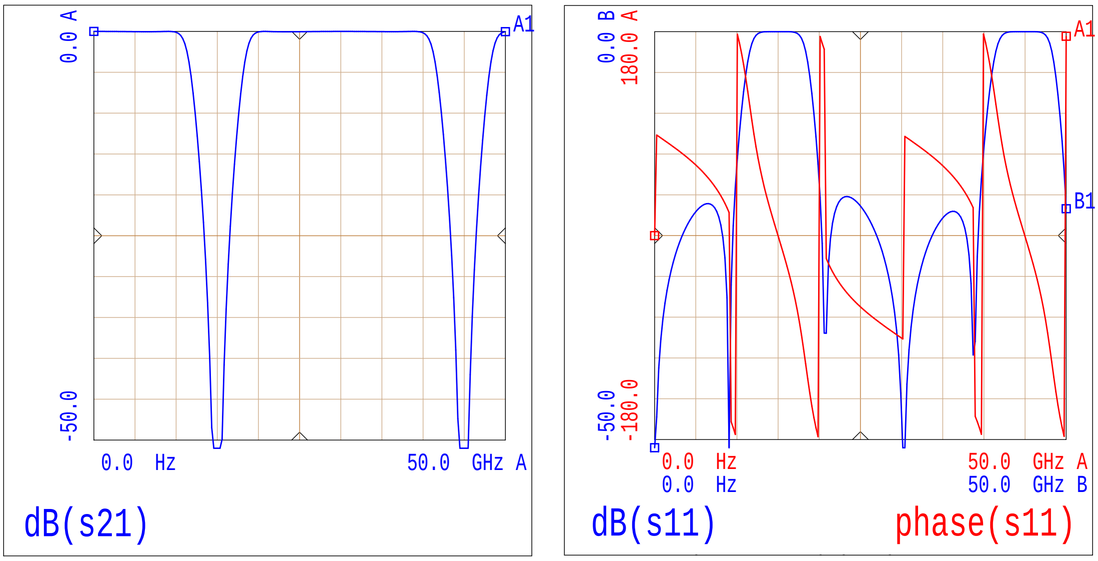

(a) (b)

Figure 45: *Transmission (a) and reflection (b) of the F0-10 low pass filter – results of the optimization*

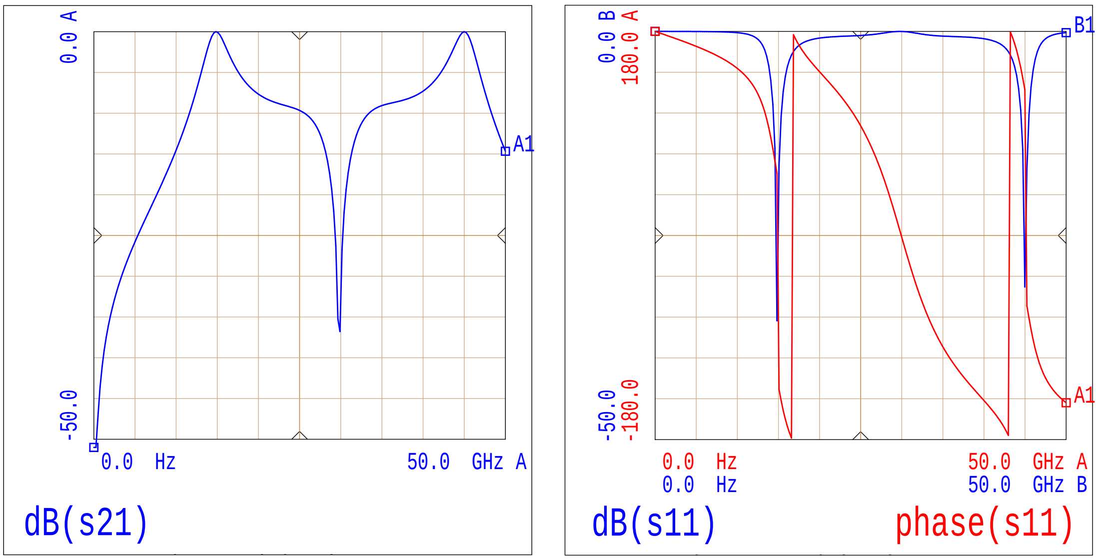

(a) (b)

Figure 46: *Transmission (a) and reflection (b) of the F15 band pass filter – results of the optimization*

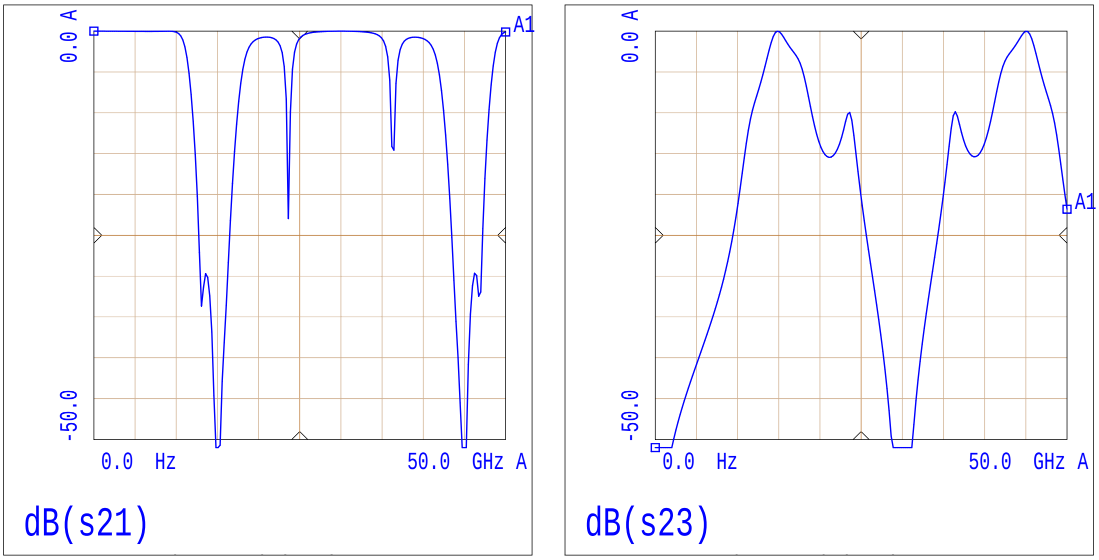

(a) (b)

Figure 47: *Transmission of the F0-10 low pass filter (a) and the F15 band pass filter (b) connected together – results of the optimization*

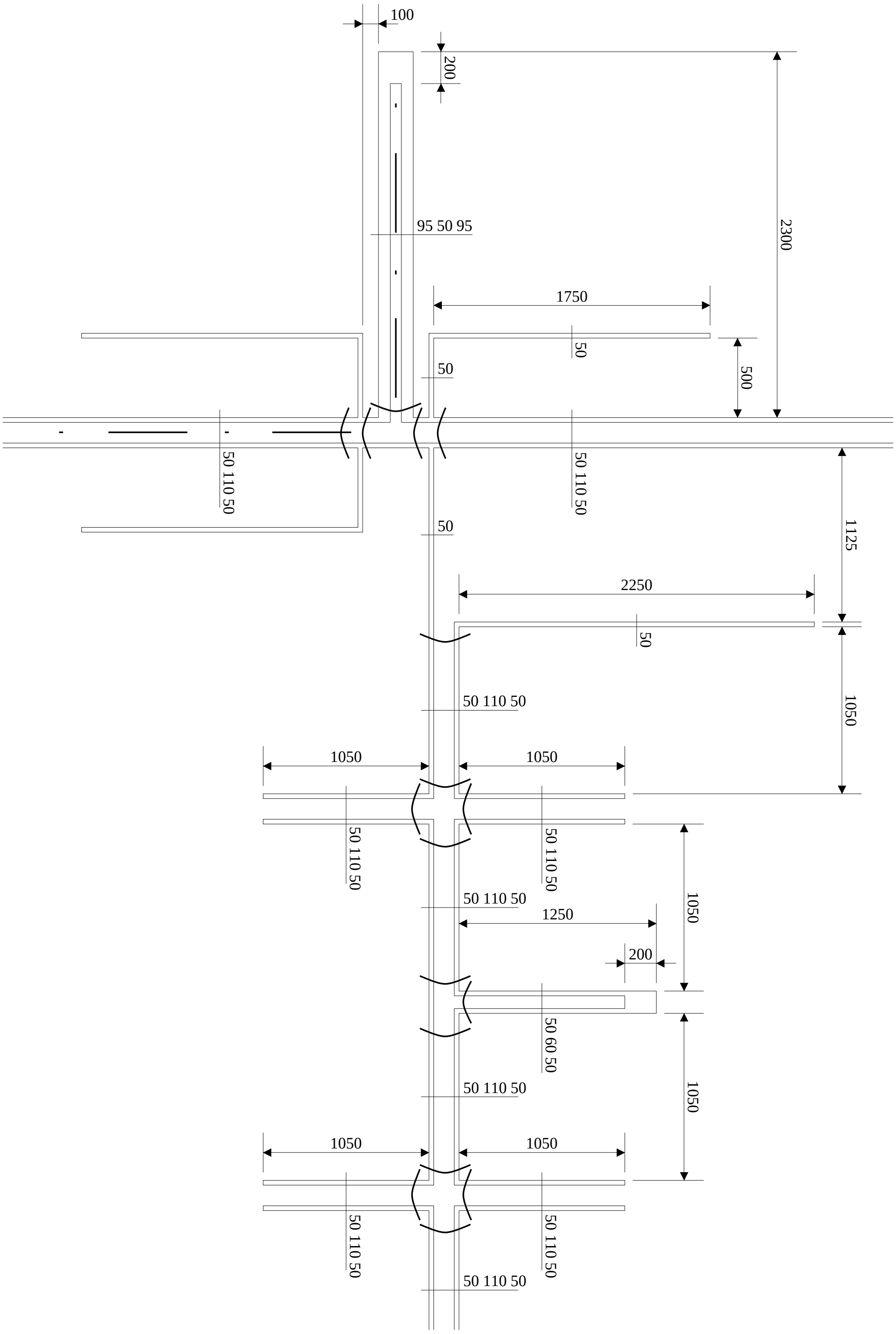

Figure 48: *The F0-10 low pass filter and the F15 band pass filter connected together – test circuit realized in the coplanar technology. Substrate: EPSILAM,* $\epsilon_r = 10.2$, $h = 635\mu m$, $t = 20\mu m$.

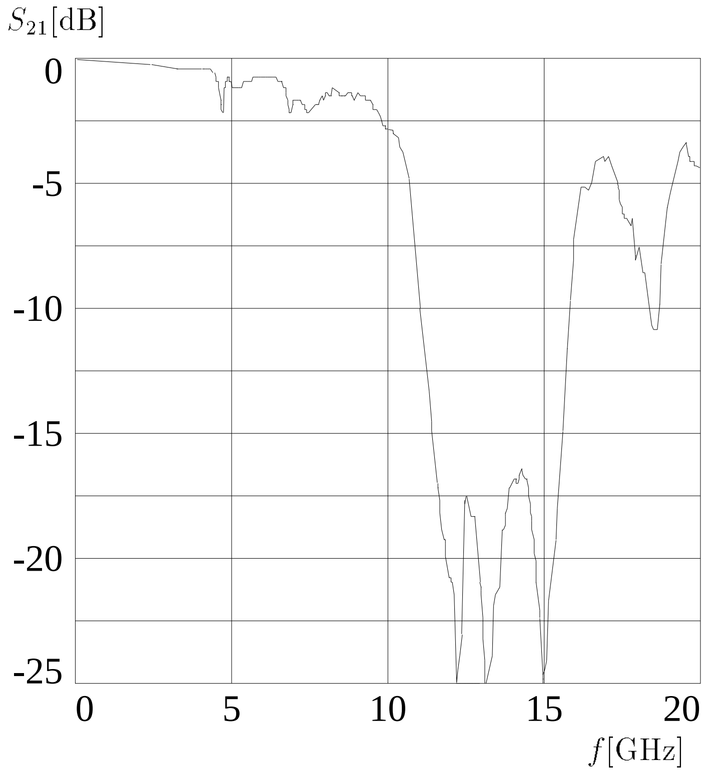

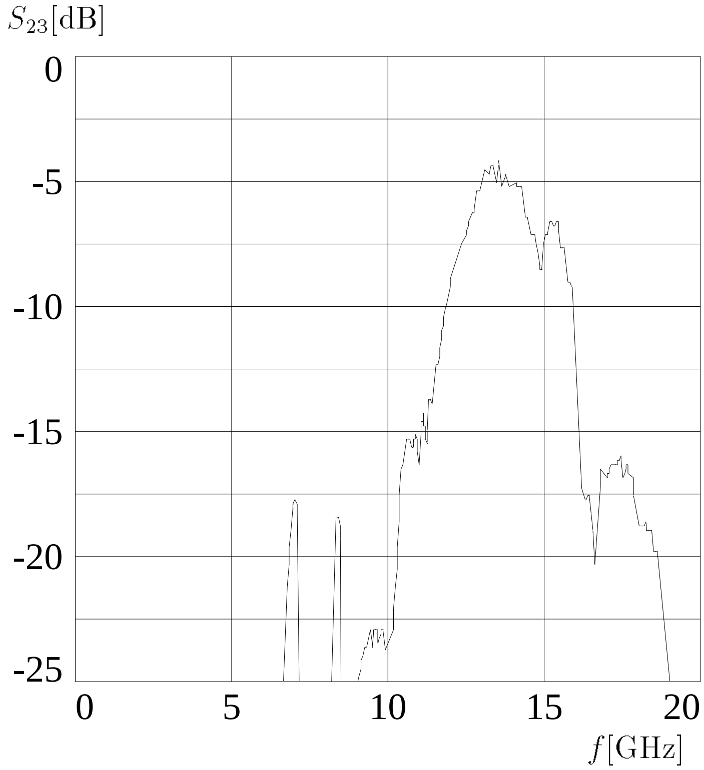

Figure 49: *Measured transmission of the F0-10 and F15 filters connected together*

4.7 Final circuit

Fig. 50, 51, 52 and 53 show all the filters designed in Sect. 4 connected together in the final circuit (compare with Fig. 35, 39 and 48). The circuit has been realized on *Alumina* substrate, $\epsilon_r = 9.9$, $h = 635\mu m$, $t = 10\mu m$. There is a place for diode connections between the F0-15 and F20-40 filters (see Fig. 12). However, because of technical problems the diodes have not been actually mounted in the circuit.

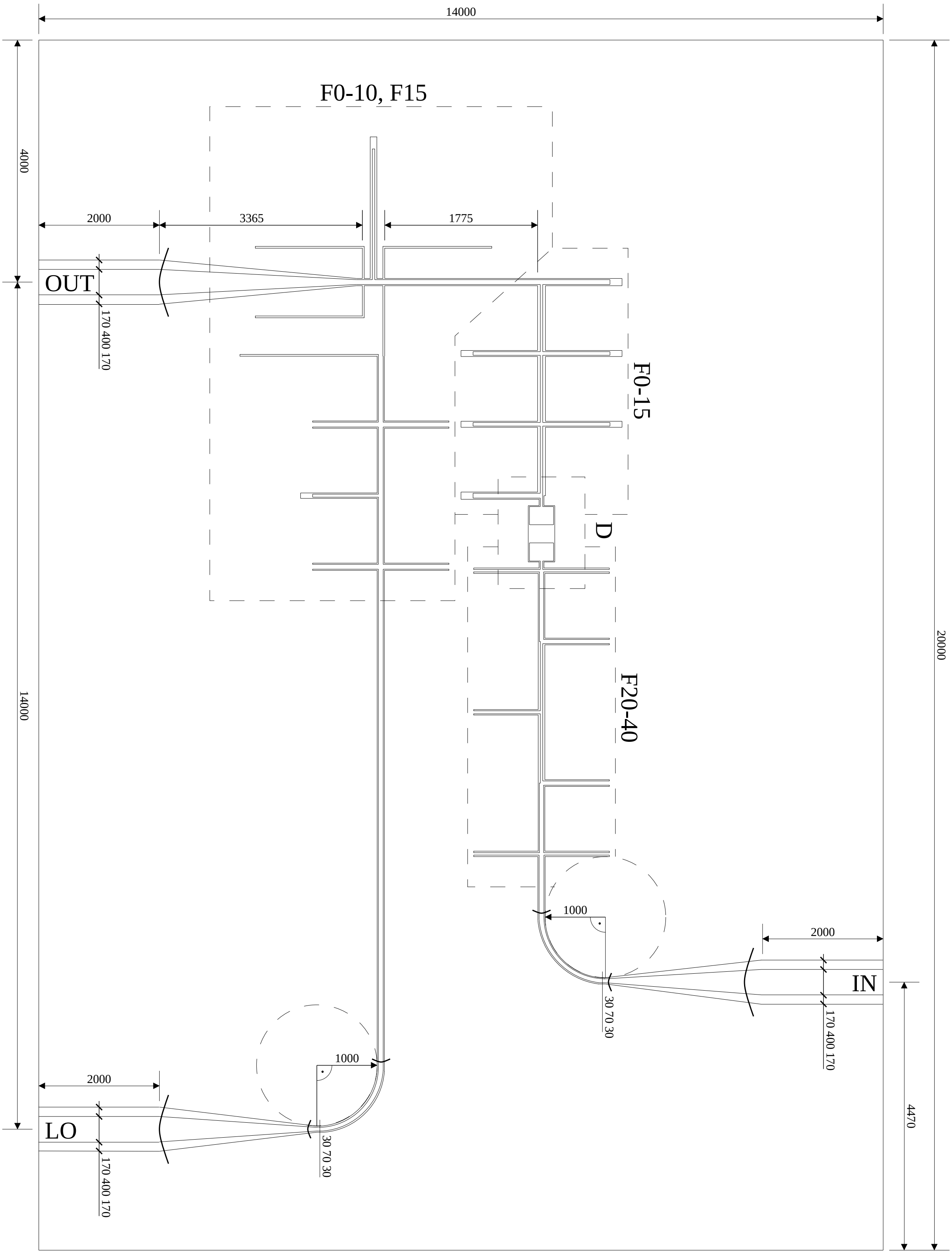

Figure 50: *All the filters in the final circuit of the mixer – realization in the coplanar technology. Substrate: Alumina, $\epsilon_r = 9.9$, $h = 635\mu m$, $t = 10\mu m$. All dimensions in μm. See details in: Fig. 51 (F0-10, F15), Fig. 52 (F0-15), Fig. 53 (F20-40), and Fig. 12 (D).*

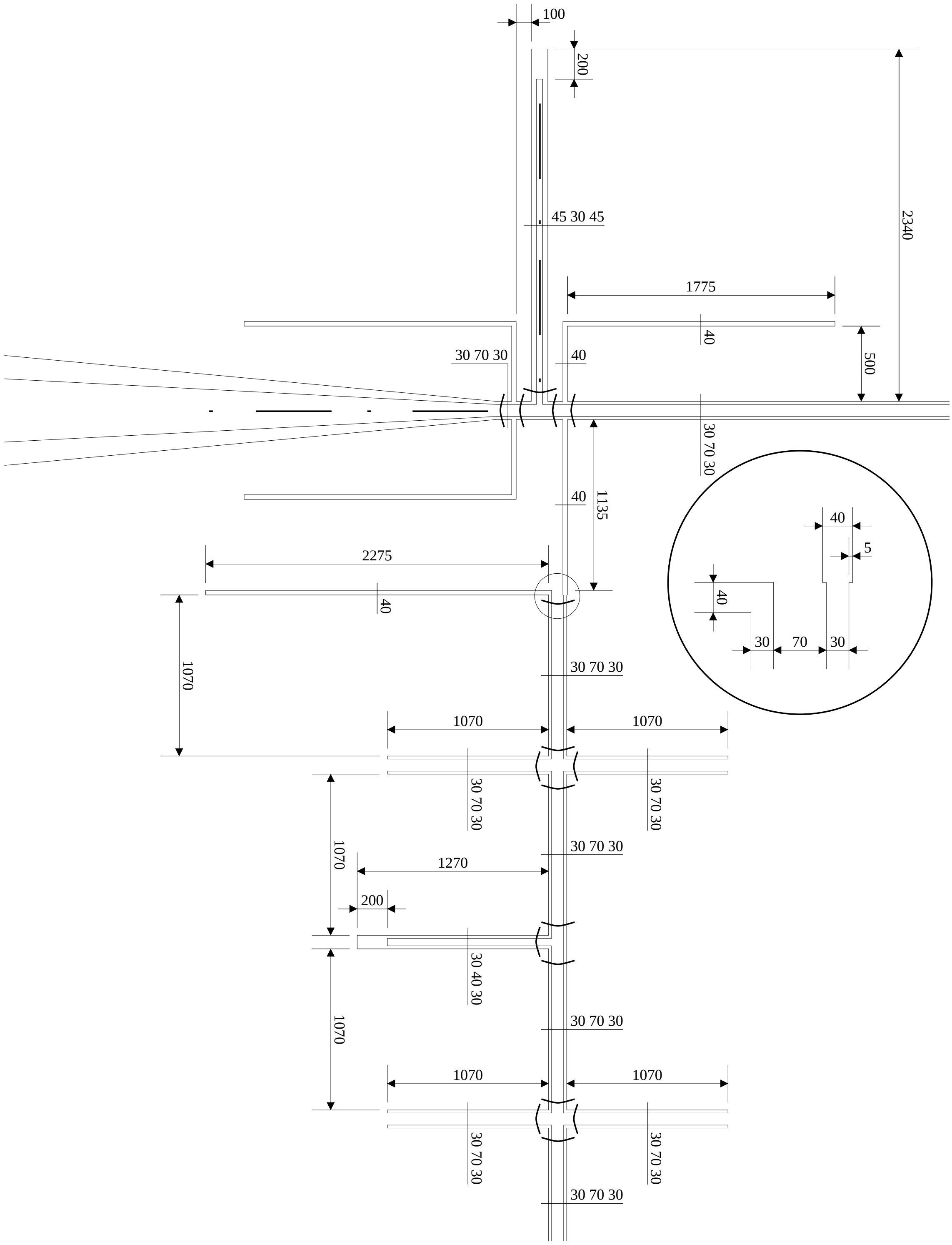

Figure 51: *The F0-10 low pass filter and the F15 band pass filter in the final circuit – detail from Fig. 50. All dimensions in μm.*

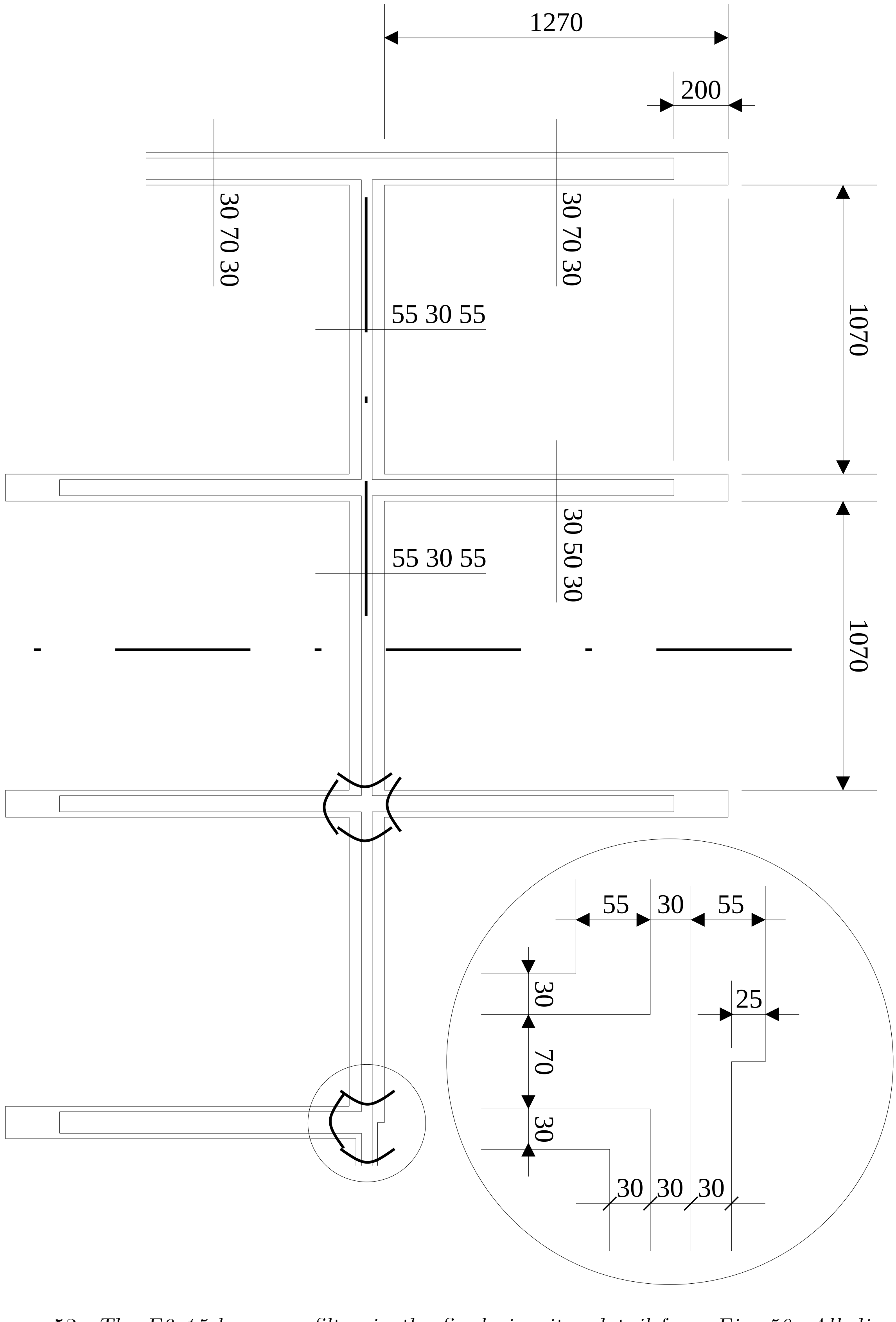

Figure 52: *The F0-15 low pass filter in the final circuit – detail from Fig. 50. All dimensions in μm.*

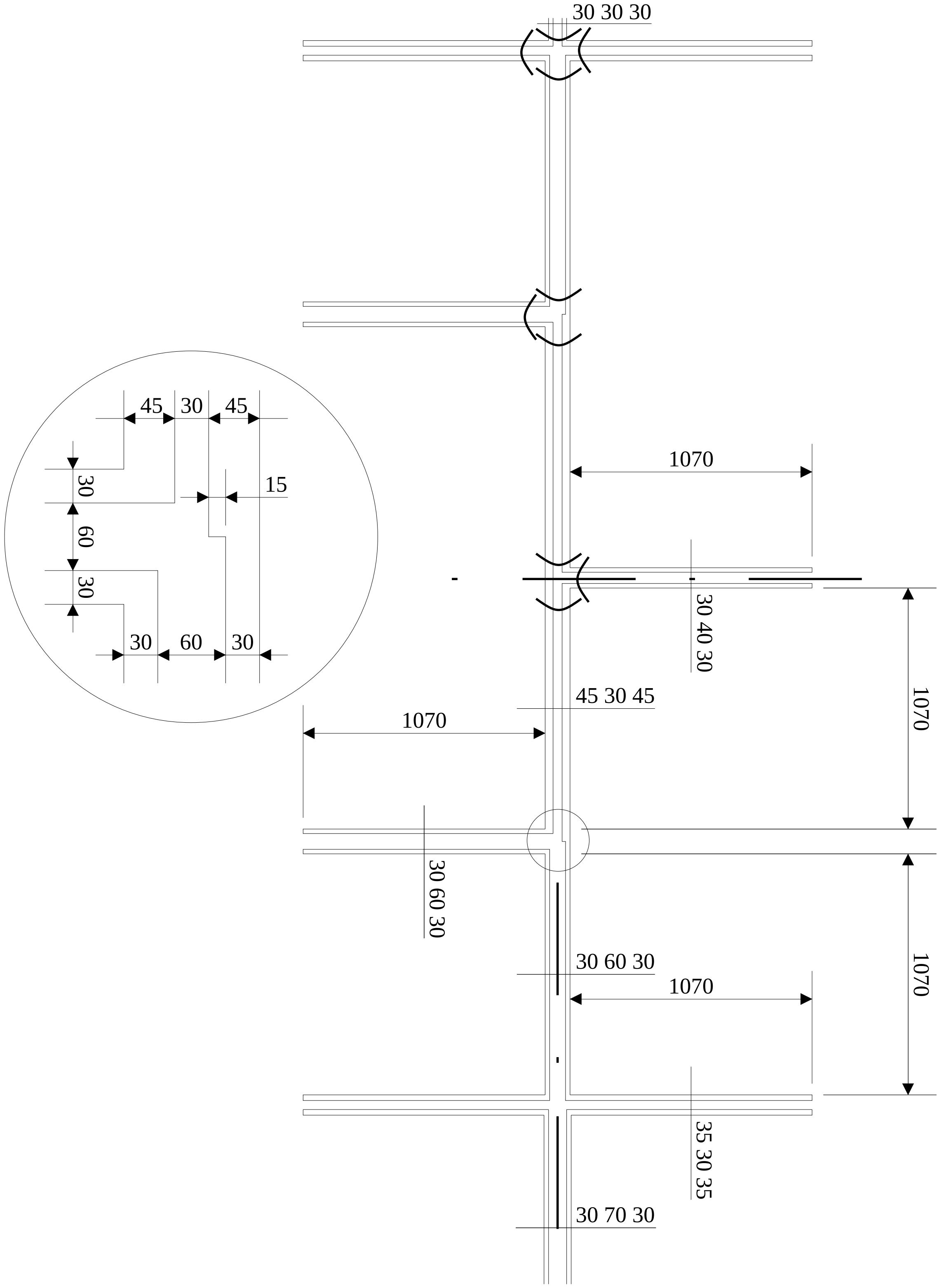

Figure 53: *The F20-40 band pass filter in the final circuit – detail from Fig. 50. All dimensions in μm.*

5 Conclusions

Design of a subharmonically pumped K band mixer with an anti-parallel pair of diodes has been presented. The nonlinear-linear analysis of the circuit gave conditions for the filter design. The filters have been designed in a uni-planar technology on the following substrates: *Alumina*, $\epsilon_r = 9.9$, $h = 635\mu m$, $t = 10\mu m$, and *EPSILAM* $\epsilon_r = 10.2$, $h = 635\mu m$, $t = 20\mu m$. Distributed elements have been used and modelled with ideal transmission lines, without considering the influence of discontinuities and dispersion. This is justified by the choice of the optimal transmission line impedance ranges for which the transverse dimensions of the lines were minimal for both substrates. Measurements have been limited to the absolute values of S_{11} and S_{21} coefficients only. The results have shown very good agreement between simulation and measurements of the filters in the frequency band 0-40GHz.

Acknowledgments

I would like to express my thanks to Dr Jerzy Chramiec for supervising this project and Jean Philippe Coupez who supervized it at the *Ecole Nationale Supérieure des Télécommunications de Bretagne*, in Brest. I would also like to thank everybody else from the *Technical University of Gdańsk* and the *ENSTB* who helped me in the realization of this project. I am indept to Dr Michał Mrozowski for his remarks and proofreading of this thesis.

References

[1] *2755/2755P Spectrum Analyzers.* TEKTRONIX, 1988

[2] Maas S. A. *Microwave mixers.* Artech House, 1986

[3] Chramiec J., Wojtkiewicz A. *Mikrofalowe mieszacze diodowe.* WKŁ1975, Warszawa

[4] Rayit A. K., McEwan N. J. *Coplanar waveguide filters.* IEEE MTT-S Digest, 1993, pp. 1317–1320

[5] Hettak K., Coupez J. Ph., Rius E. and Toutain S. *A new uniplanar bandpass filter using $\lambda_g/2$ slotline and $\lambda_g/4$ coplanar waveguide resonators.* ENST de Bretagne – Université de Bretagne Occidentale

[6] Hettak K., Le Gouguec T., Coupez J. Ph., Toutain S., Meyer S. and Penard E. *Very compact low-pass and band-pass filters using uniplanar structures.* ENST de Bretagne